ELSEVIER

Chemical Geology 182 (2002) 139–178

CHEMICAL GEOLOGY
INCLUDING
ISOTOPE GEOSCIENCE

www.elsevier.com/locate/chemgeo

The cretaceous Ladakh arc of NW himalaya—slab melting and melt–mantle interaction during fast northward drift of Indian Plate

Yann Rolland [a,*], Christian Picard [a,b], Arnaud Pecher [a], Henriette Lapierre [a], Delphine Bosch [c], Francine Keller [a]

[a] *LGCA, UMR-A5025 CNRS-Université Joseph Fourier, Maison des Géosciences, 1381 rue de la piscine, BP 53, 38041 Grenoble, France*
[b] *Université de Nouvelle Calédonie, BP 4477, Géosciences, 98847 Nouméa, Nouvelle Calédonie, France*
[c] *Laboratoire de Tectonophysique, CNRS UMR-5568, Université de Montpellier II, Place E. Bataillon, 34095 Montpellier Cedex 05, France*

Received 27 June 2000; accepted 10 March 2001

Abstract

The Kohistan–Ladakh Terrane in the NW Himalaya is a remnant of a Cretaceous arc sequence obducted onto the Indian margin. This paper presents a geochemical study (major and trace elements and Sr, Nd, Pb isotopes) of the Mid-Cretaceous lavas of the Ladakh side of the arc sequence, which were erupted in response to northward subduction of Neo-Tethys oceanic crust.

Lavas from the western Ladakh in Pakistan can be divided into three groups which, from north to south, are: (1) the Northern Group of back-arc tholeiites [$0.5 < (La/Yb)_N < 1.4$; $0.3 < (Nb/La)_N < 1.4$; $4 < \varepsilon Nd < 8$; $38.66 < {}^{208}Pb/{}^{204}Pb < 38.80$], (2) the Southern Group of arc tholeiites [$1.8 < (La/Yb)_N < 3.9$; $0.1 < (Nb/La)_N < 0.6$; $5 < \varepsilon Nd < 6$; $38.40 < {}^{208}Pb/{}^{204}Pb < 38.66$], and (3) the Katzarah Formation of tholeiitic Nb-rich lavas [$3.4 < (La/Yb)_N < 9.8$; $1.4 < (Nb/La)_N < 2.1$; $3 < \varepsilon Nd < 5$], including radiogenic Pb lavas [$39.31 < {}^{208}Pb/{}^{204}Pb < 39.51$] and less radiogenic lavas [$38.31 < {}^{208}Pb/{}^{204}Pb < 38.55$]. Magmas from the eastern Ladakh in India show a simple series of more evolved arc volcanics from basalts to rhyolites [basalts and basaltic andesites: $2.5 < (La/Yb)_N < 5.7$; $0.4 < (Nb/La)_N < 0.5$; $1.8 < \varepsilon Nd < 5.5$; $38.70 < {}^{208}Pb/{}^{204}Pb < 38.80$]. Isotope and trace element data of western Ladakh lavas are compatible with high-degree melting (14–21%) of a fertile MORB-mantle source. An adakitic lava [$(La/Yb)_N = 55.8$; $(Nb/La)_N = 0.3$; $\varepsilon Nd = 1.7$; ${}^{208}Pb/{}^{204}Pb = 39.00$] and a Mg-poor Nb-rich basalt [$(La/Yb)_N = 4.6$; $(Nb/La)_N = 1.3$; $\varepsilon Nd = -2$; ${}^{208}Pb/{}^{204}Pb = 39.07$] are spatially associated with the tholeiitic arc lavas. Isotope compositions of all the lavas, and in particular the radiogenic Nb-rich and adakitic lavas suggest three-component mixing between depleted mantle similar to the Indian MORB mantle, and enriched components similar to the volcanogenic or pelagic sediments. The geochemical diversity of magma types is attributed to contribution of melts from the subducted crust and associated sediments, and their subsequent interaction with the mantle. Such melt–mantle interactions can also be inferred from relicts of sub-arc mantle found in Indian Ladakh. These results lead to a geodynamic reconstruction of the Kohistan–Ladakh arc as a single entity in the Mid-Cretaceous, emplaced south of the Asian margin. Slab melting imply subduction of young oceanic crust, as already proposed for the Oman ophiolite farther west. The fast northward drift of the Indian Plate could have triggered wide-scale inversion of the divergent tectonic regime

* Corresponding author. Fax: +33-4-7682-8070.
E-mail address: yrolland@ujf-grenoble.fr (Y. Rolland).

PII: S0009-2541(01)00286-8

responsible for the opening of the Neo-Tethys Ocean. Our results suggest breaking of the young oceanic crust initiated at the ridge rather than at passive plate boundaries.

Keywords: Ladakh; Island arc; Back-arc; Crustal melting; Nd Sr and Pb isotopes

1. Introduction

Since Permian times, complex tectonic disturbances, involving closure of oceanic domains, crustal aggregation and mountain building occurred in the peri-Tethys realm to form the present day Himalayan mosaic. One puzzling problem concerns the origin and initial geodynamic setting of some parts of this

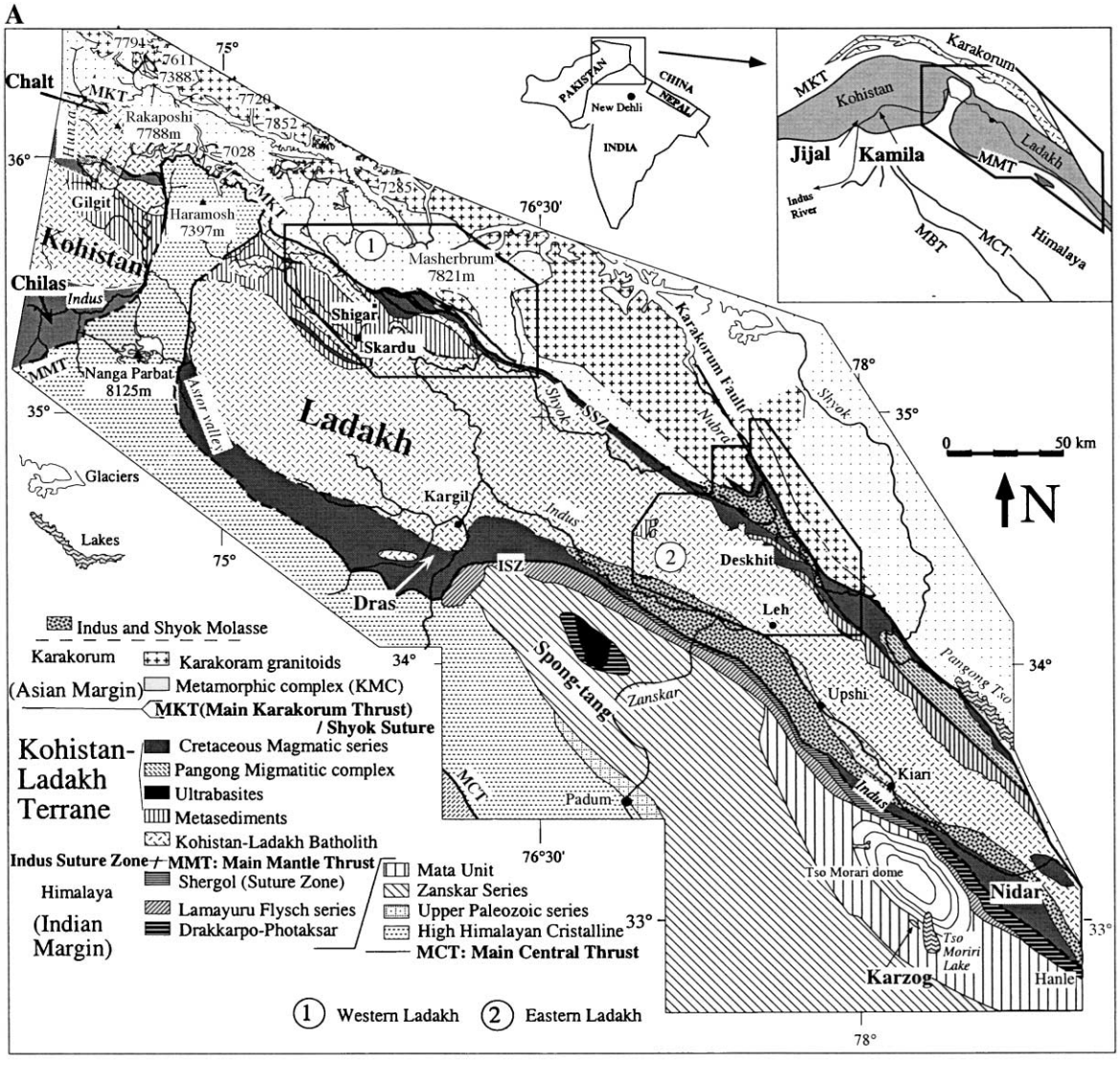

Fig. 1. Geological setting of the Ladakh series. (A) General geological map of the Ladakh Terrane. (B) Enlarged (simplified) geological maps of (1) Western and (2) Eastern Ladakh areas, with REE normalised patterns of representative lavas from each geological unit. Normalisation values are from Evensen et al. (1978).

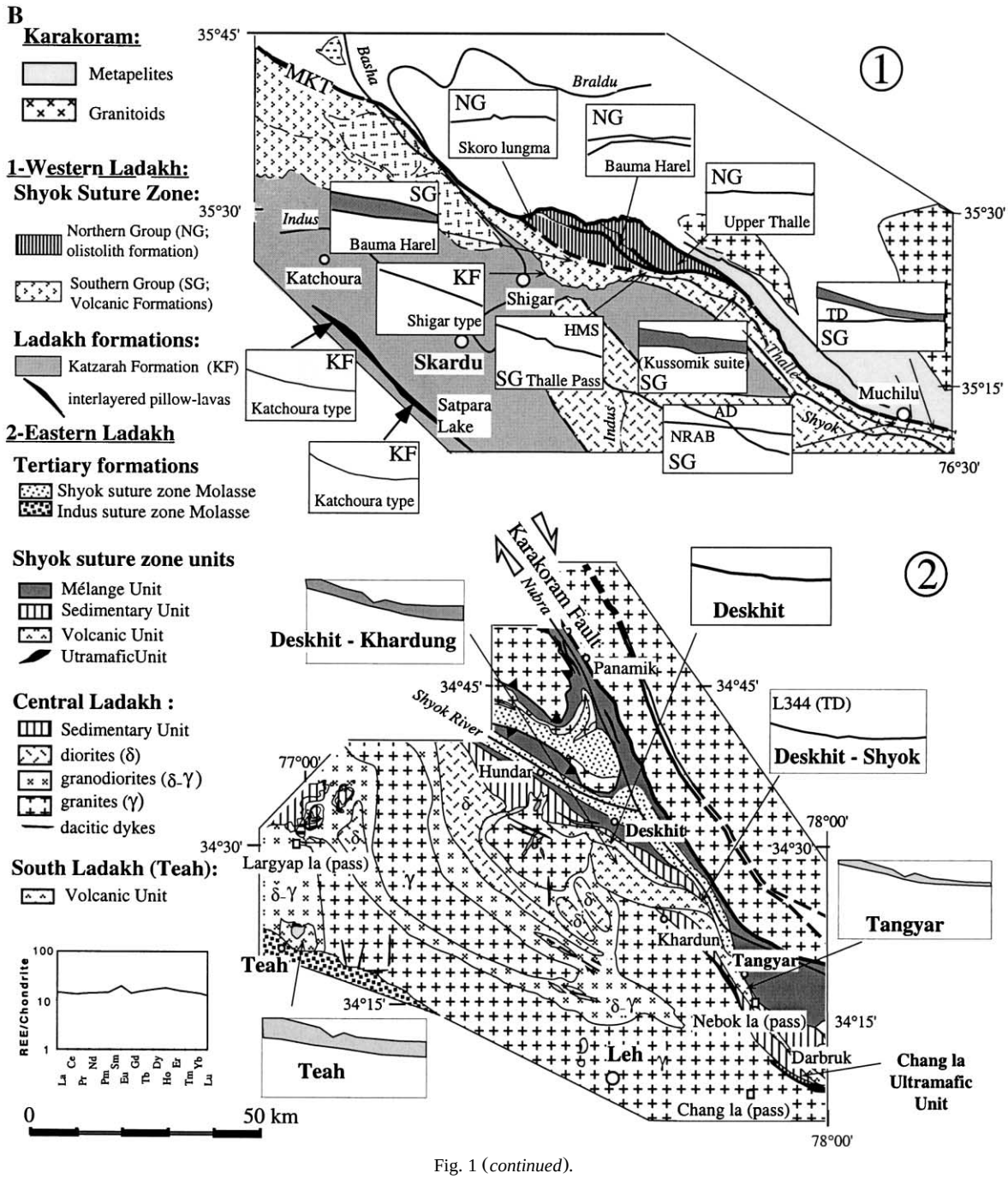

Fig. 1 (*continued*).

mountain belt. Among these, the geodynamic evolution of the Kohistan–Ladakh Terrane (Fig. 1A) in the Mid-Cretaceous times remains poorly understood. The Albian–Cenomanian Kohistan–Ladakh arc-series were built somewhere between the Indian and Asian plates in response to the subduction of the

Neo-Tethys Ocean during the fast northward drift of the Indian plate. The series are thought to have been emplaced either above a north dipping subduction zone, in an intra-oceanic context, close to the Asian margin (Tahirkeli et al., 1979; Bard et al., 1980; Thakur and Misra, 1984; Khan et al., 1996; Treloar et al., 1996), or above a south dipping subduction zone, in the oceanic zone of the Dupal anomaly, about 3000 km to the south of its present position (Khan et al., 1997). At present, it is still difficult to understand whether and how the Kohistan–Ladakh arc was connected to the Tibetan Asian continental arc (Lhasa Block), a region in which there is no evidence of oceanic arc or back-arc basin formations (Coulon et al., 1986). West of Ladakh, the Kohistan arc has generally been interpreted as a unique arc (Bard et al., 1980; Tahirkeli, 1982), but it is possible that more than one arc system existed in view of the wide initial oceanic realm separating Asia and India in the Lower Cretaceous and to the long time-span of convergence before collision (Lower Cretaceous–Eocene). Located between the Kohistan intra-oceanic arc and the Tibetan continental arc-series, the Ladakh region represents a key area for a better understanding of the geodynamic situation of the Asian margin and Indian Tethyan arc-systems in the Mid-Cretaceous times.

In a previous paper (Rolland et al., 2000), we presented the geochemical features of the igneous components of the Northern Ladakh Terrane and proposed that during the Mid Cretaceous, (i) a narrow back-arc basin was present, ending progressively into Eastern Ladakh, and (ii) the Eastern Ladakh lavas developed in an active margin setting with close similarities to the Tibetan continental arc-rocks. This implies that the intra-oceanic Kohistan–Western Ladakh arc probably evolved laterally towards an Andean-type margin in Tibet and that this evolution could be likely related to an oblique subduction of the Neo-Tethys ocean along the Asian margin.

In this paper, we present new trace element and isotopic geochemical data on lavas from the Indo-Pakistanis Ladakh, sampled in two areas (Fig. 1A,B): (1) the Skardu area in Pakistan Ladakh (Western Ladakh), and (2) the Nubra-Shyok and Teah areas in India or Eastern Ladakh. These new data allow better constraints on the geodynamic evolution of the Indo-Pakistanis Ladakh arc in Mid-Cretaceous times. These data are expected to provide new insights in the petrological processes related to the fast northward drift of the Indian Plate and its geodynamic implications for the peri-Tethyan margins.

2. Geological setting

The Ladakh Terrane, located in both north–east Pakistan and north–west India, is bounded to the north by the Northern or Shyok suture zone, and to the south by the Indus suture zone (Fig. 1A). The Ladakh series are interpreted as remnants of a wide volcanic arc separated from its western Kohistan pendant by the Nanga Parbat–Haramosh spur. The arc developed as a consequence of the northward subduction of the Neo-Tethys Ocean along the Indus suture zone (Tahirkeli et al., 1979; Honegger, 1983). Arc-volcanism began during the Mid-Cretaceous, as suggested by Rb–Sr and Ar–Ar ages of 110 and 90 Ma, both obtained in Ladakh (Schärer et al., 1984) and Kohistan (Treloar et al., 1989; Mikoshiba et al., 1999). These ages have been confirmed by palaeontological associations of Albian–Aptian age in both Kohistan and Ladakh (Desio, 1974; Tahirkeli, 1982; Dietrich et al., 1983; Pudsey, 1986; Reuber, 1989; Rolland et al., 2000).

According to Khan et al. (1997), all the rocks of the Kohistan arc are contemporaneous and represent different parts of an arc–back-arc system. The Kamila amphibolites were emplaced in the back-arc basin while the Chalt boninites and the Chilas lavas represent the fore-arc and arc, respectively. For Treloar et al. (1996), these different formations succeeded in time, Kamila amphibolites being the basement of the arc.

According to various authors, the Ladakh Mid-Cretaceous volcanic and plutonic rocks (Dras, Spontang, Nidar) belong to an arc developed above a north dipping subduction zone (Reibel and Juteau, 1981; Honegger et al., 1982; Dietrich et al., 1983; Maheo et al., 2000). These arc-formations are intruded by large granodioritic plutons in Ladakh (De Terra, 1935; Dietrich et al., 1983; Honegger, 1983; Raz and Honegger, 1989), as in Kohistan (Tahirkeli et al., 1979; Bard et al., 1980; Petterson and Windley, 1985). The earliest intrusions are, as the lavas, Middle Cretaceous in age. Ages of 101–103 Ma

were obtained in Ladakh (U–Pb ages from Honegger et al., 1982; Schärer et al., 1984), while ages of ~100 Ma were obtained in Kohistan [102 Ma (Rb–Sr) by Petterson and Windley, 1985 and 97–99 Ma (U–Pb) by Schaltegger et al., 2000]. Igneous rocks from Kohistan and Ladakh display then similar geochemical features (Petterson and Windley, 1991; Sullivan et al., 1994; Shah and Shervais, 1999; Ahmad et al., 1998). An important plutonic activity lasted until 25 Ma, with successive emplacement of more and more differentiated granitoid intrusions. The geochemical affinities of these plutons indicate that the Kohistan–Ladakh arc Terrane evolved as an active margin after its accretion to the Asian plate (Petterson and Windley, 1991; Treloar et al., 1996). The structures of the Kohistan–Ladakh arc are now obscured by the post accretion plutonism and tectonism. Hence, relicts of the former Cretaceous volcanic products of the arc are rare and mainly preserved in north-eastern Kohistan, and in northern and southern Ladakh.

Rolland et al. (2000) have distinguished two different units in the Western Ladakh rocks along the Shyok Suture Zone (Skardu area, north–east Pakistan, 1 in Fig. 1A and B): (1) the Northern Group with volcanic and sedimentary rocks emplaced in a back-arc basin, and (2) the Southern Group composed of arc tholeiites. The Northern and Southern Groups are separated by irregular and curved contacts, limited by ultramafic serpentinised rocks. South of the Shyok Suture Zone, the Katzarah Formation consists of metapelitic rocks and rare OIB-type pillow-lava interlayers. The tectonic stacking of these units is contemporaneous to an amphibolite grade metamorphism caused by the northward subduction of the arc and back-arc basin sequences under the Karakoram continental margin during the Late Cretaceous (Rolfo et al., 1997; Rolfo, 1998).

In Eastern Ladakh, along the Shyok Suture Zone (north–west India; 2 in Fig. 1A and B), four units have been recognised (Rolland et al., 2000), which are from north to south.

(i) The "Mélange Unit" is exposed in the Nubra valley and Pangong Range and is composed of deformed volcano-sedimentary formations in which metapelites represent the most abundant lithology (Rai, 1983).

(ii) The "Sedimentary Unit" consists of a thick pile of Aptian–Albian sandstones with minor limestone beds, interlayered in its upper part with basaltic and andesitic flows.

(iii) The "Volcanic Unit" overlies the previous unit and consists of a thick sequence of arc-volcanic rocks starting with basalts and andesites and finishing up with dacitic and rhyolitic ignimbrites.

(iv) The "Chang La Ultramafic Unit", in tectonic contact with the Volcanic Unit, is composed of harzburgites and gabbros, well preserved north of the Chang La pass (Reuber, 1990).

The sedimentary lithologies associated with the volcanic rocks are indicative of a west–east evolution from a marine, carbonated environment in Western Ladakh to a continental, silico-clastic, environment in Eastern Ladakh. In Western Ladakh, lithologies and geochemistry of volcanic rocks (Fig. 1B) show a north–south evolution from a pristine back-arc basin to an intra-oceanic arc: the Northern and Southern Groups, respectively. The back-arc basin likely ends in Eastern Ladakh, where the lavas are more differentiated and homogeneous in composition. These data suggest that the intra-oceanic Western Ladakh evolves eastwards towards a more mature arc (Eastern Ladakh) which is probably in continuity with the Lhasa block (Tibetan) active continental margin.

3. Analytical procedures

Mineral analyses (presented in Table 1) were obtained on a Cameca SX-100 microprobe at the University Blaise Pascal of Clermont-Ferrand. Counting time was 10 s per element, the accelerating potential was 20 kV for a sample current of 20 nA. Natural silicates were used as standards.

Major element abundances of Western Ladakh lavas have been obtained using an Inductively Coupled Atomic Emission Spectrometer (ICPAES). Major element data of Eastern Ladakh lavas has been obtained using X-Ray fluorescence at the University C. Bernard of Lyon. Trace element abundances were measured using inductively coupled plasma mass

spectrometry (ICP-MS) at the University Joseph Fourier of Grenoble. Samples selected for major element analysis by ICPAES and trace elements by ICPMS were attacked using a microwave heater. Most acid samples ($SiO_2 > 60$ wt.%) and adakitic sample L65 were attacked in a bomb™ at 350°C for 5 days. Solution trace element abundances were measured by ICP-MS following procedures described by Barrat et al. (1996). Trace elements were spiked with pure Tm, which was used as internal standard. Major, trace and REE data are presented on Table 2. Errors on measurements obtained from nine runs of BHVO standard are given at 2σ% on Table 2. Loss on ignition (LOI) was determined by heating the sample at 1000°C for 30 min.

Chemical separation of Sr and Nd was carried out at Joseph Fourier University following the analytical procedures of Lapierre et al. (1999). Samples were leached in HCl 6N after dissolution and prior to REE separation. Dissolution of ~0.1 g of samples was realised in closed teflon screw cap vessels with a HF-HNO_3 mixture, converted to chlorine form using HCl. Chemical separation of Sr was carried out on a AG50W (200–400 mesh) cationic ion exchange column. Nd separation was carried out using (1) exchange reverse chromatography AG50WX8 cationic ion exchange column followed by (2) H_2HP orthophosphoric column separation. The Nd and Sr isotopic data ($^{143}Nd/^{144}Nd$ and $^{87}Sr/^{86}Sr$ isotopic compositions) were measured on a Finnigan MAT261 multicollector mass spectrometer at the Geochemical Laboratory, Paul Sabatier University of Toulouse. $^{87}Sr/^{86}Sr$ was normalised to 8.3752, NBS standard was measured to 0.710250 (±15). $^{143}Nd/^{144}Nd$ ratio was normalised to a value of $^{146}Nd/^{144}Nd$ of 0.71219; measure of Rennes standard was 0.511965 (±12).

The chemical separation of lead was done at the Geochemical Laboratory of Montpellier University following a procedure modified from Manhès et al. (1978). Total Pb blanks were less than 65 pg for 100 mg. The Pb isotopic ratios were measured on the MC-ICP-MS P54 at the Ecole Normale Supérieure (E.N.S) of Lyon. Isotopic Pb values of NBS standard were measured to: $^{208}Pb/^{204}Pb = 36.69035$; $^{207}Pb/^{204}Pb = 15.49303$; $^{206}Pb/^{204}Pb = 16.95323$. Errors on measurements, obtained from five runs of NBS standard are of 0.02 for $^{208}Pb/^{204}Pb$, of 0.007 for $^{207}Pb/^{204}Pb$, and 0.005 for $^{206}Pb/^{204}Pb$. Isotopic data are presented in Table 3.

4. Results

4.1. Petrography and mineral chemistry of the Ladakh Terrane volcanic and ultramafic rocks

In Western Ladakh (Skardu area), pillow-lavas predominate with some massive lava-flows and tuffs, and rare pyroclastic lapilli or bomb tuffs interlayers. Compositions range from basalt to andesitic basalt. Igneous assemblages have been overprinted by a medium pressure–medium temperature metamorphism. Metamorphic assemblages are albite + actinolite blue-green amphibole + calcite ± epidote ± chlorite ± biotite, recrystallised in replacement of primary pyroxene and plagioclase. Nevertheless, the magmatic minerals can be recognised through the nature of the recrystallising metamorphic assemblage and preservation of the initial textures. Thin-grained tuffs or aphanitic lavas have been totally recrystallised, but most lavas are phyric and present relicts of plagioclase, pyroxene and more rarely amphibole, generally defining an intersertal to glomerophyric texture.

In Eastern Ladakh (Nubra-Shyok and Teah areas, on both sides of the Ladakh Batholith), a minor proportion of volcanic rocks has escaped from metamorphic recrystallisation, regionally of greenschist grade (Rai, 1983). The metamorphic assemblage consists of epidote + calcite ± actinolite. The lavas range from basalts to rhyolites. Pyroxene + plagioclase + spinel is the main assemblage of basalt and basaltic andesites. In the andesites, centimetre-sized large plagioclase phenocrysts predominate with minor oxides and rare clinopyroxene, defining an intersertal texture. In the dacites, most phenocrysts are albitic plagioclase and rare quartz. Pyroxene is absent. Texture is mostly ignimbritic, with minor proportions of glass. In the rhyolites, abundant clasts of quartz and K-feldspar and scarce clasts of albite and biotite define clastic and sometimes welded ignimbritic textures.

Unaltered phenocrysts are present in only few basaltic andesites of the Nubra-Shyok area. Therefore mineral analyses of the more differentiated lavas

have not been possible. Mineral analyses of basaltic andesite lavas are presented in Fig. 2. Plagioclase is Ca-rich with frequent increase of the anorthite content from core to rim (An = 0.4–0.8), defining an inverse zoning (Fig. 2A). Spinel is a Ti-rich ulvöspinel. Pyroxenes display diopsidic to augitic compositions (a in Fig. 2B), with frequent inverse zoning, defined by the increase of enstatite correlated with a decrease of ferrosillite contents from core to rim. Most Ladakh pyroxenes (this study and Dietrich et al., 1983) plot in the orogenic and alkaline fields of Leterrier et al. (1982) (b in Fig. 2B). However, the compositions of Eastern Ladakh pyroxenes appear to be more tholeiitic and closer to the non-orogenic fields than southern Ladakh (Dras) pyroxenes of Dietrich et al. (1983).

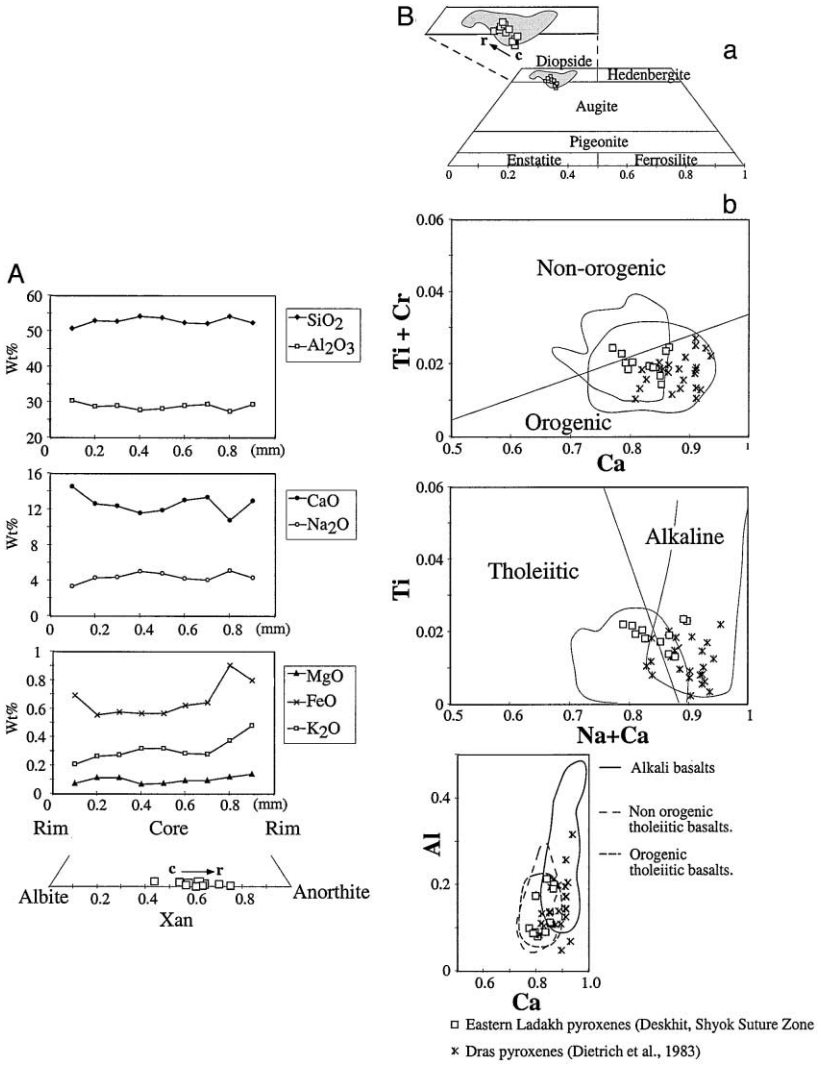

Fig. 2. Mineral chemistry of Eastern Ladakh basaltic andesites. (A) Composition of plagioclase in the albite–anorthite–(orthose) diagram, and profiles of a single plagioclase grain. (B,a) Composition of pyroxene in the enstatite–ferrossilite–(wollastonite) diagram; and (B,b) pyroxene plots in discrimination diagrams of Leterrier et al. (1982). In the discrimination diagrams, using the cations Ca vs. Ti + Cr, Na + Ca vs. Ti and Ca vs. Al, the fields represent 5% level confidence for alkali and calc-alkali basalt data compiled by Leterrier et al. (1982). Eastern Ladakh pyroxenes are compared to Dras pyroxenes of Dietrich et al. (1983).

The Chang La Ultramafics are exposed north of the Chang La pass in Eastern Ladakh (2 in Fig. 1B). Peridotites (mainly dunites) are composed of triple-jointed 80–90% olivine, 5–10% of irregular and elongated orthopyroxene and 3–5% of large (0.1–0.5 mm) and isolated spinel grains (clinopyroxene has not been observed). Minerals have tight compositional ranges, shown in Table 1. Olivine is Mg-rich (Fo: 93.7–94.2), orthopyroxene is also Mg-rich (En: 89.8–91.6) and Al_2O_3-poor (0.9–1.6%), spinel has very high Cr# ($Cr/(Cr + Al) = 0.85$) and low Mg# ($Mg^{2+}/(Mg^{2+} + Fe^{2+}) = 0.2–0.4$; Table 1).

Table 1
Representative mineral analyses of Chang La ultramafics

	Orthopyroxene $n = 3$		Olivine $n = 8$		Spinel (rim) $n = 1$	Spinel (core) $n = 6$
SiO_2	57.7		41.5		0.1	–
Al_2O_3	1.2		–		3.0	4.1
MgO	36.3		52.5		–	6.5
FeO	4.1		5.8		71.5	47.2
Fe_2O_3	1.0		–			–
MnO	0.2		0.1		1.4	0.3
Cr_2O_3	0.1		–		0.1	38.6
TiO_2	–		–		17.4	–
NiO	–		0.4		–	0.3
CaO	0.1		–		–	–
Na_2O	–		–		–	–
K_2O	–		–		–	–
Total	100.6		100.3		93.4	97.0
						0
Nb. Oxy.	6.0		4.0		32.0	32.0
Si	2.0		1.0		–	–
Al	0.0		–		1.0	1.4
Ti	–		–		3.7	–
Fe^{3+}	0.0		–		11.2	5.8
Fe^{2+}	0.1		0.1		5.8	5.4
Mg	1.9		1.9		–	2.7
Ca	–		–		–	–
Mn	–		–		0.3	0.1
Cr	–		–		–	8.6
Ni	–		–		–	0.1
Na	–		–		–	–
Jadeite	2.1	Fo	94.0	Mg#	–	0.3
Woll.	0.2			Cr#	–	0.9
Ens.	91.0					
Ferro.	6.8					

Woll: wollastonite; Ens: enstatite; Ferro: ferrosilite; $Mg\# = Mg/(Mg + Fe^{2+})$; $Cr\# = Cr/(Cr + Al)$.

We have used the following reaction for the calculation of temperature and oxygen fugacities ($\Delta \log fO_2$): $6Fe_2SiO_4$ (olivine) + $O_2 = 3Fe_2Si_2O_6$ (orthopyroxene) + $2Fe_3O_4$ (Spinel), from the calibrations of Nell and Wood (1991) and Balhaus et al. (1991). Temperature calculations of 1100 ± 30°C are obtained at a nominal pressure of 13 kbar (mean pressure value of spinel-bearing mantle field at $T \sim$ 1100°C; Jaques and Green, 1980). Accurate $\Delta \log fO_2$ calculations depend on the determination of the ferric iron content of spinel, derived stoichiometrically, and are thus sensitive to errors in the measure of M^{3+} cations such as Al. Nevertheless, Wood and Virgo (1989) have argued that electron microprobe analysis yields precise enough data to obtain $\Delta \log fO_2$ values. $\Delta \log fO_2$ calculations gave high values, 2–3.3 log units above the fayalite–magnetite–quartz (FMQ) buffer.

4.2. Geochemical study of the Ladakh volcanic rocks

Thirty-one samples of Western Ladakh and 16 samples of Eastern Ladakh have been selected for major and trace element analyses. Part of the data is presented in Rolland et al. (2000), and eleven additional samples are presented in Table 2. Fifteen samples of Western Ladakh and nine samples of Eastern Ladakh were selected for Nd, Sr and Pb isotopic analyses, presented in Table 3. All these analyses are summarised in Table 4, for each geological unit.

4.2.1. Alteration, hydrothermal and metamorphic effects

In a first approach, we will investigate the mobility of Sr, Nd, Th, U and Pb, on which the isotopic study is based. Since zirconium is an incompatible element (for basaltic to andesitic lavas) that has generally been shown to remain stable during alteration or weathering processes, it has been used as reference to study the mobilities of Sr, Nd, Th, TiO_2 and Pb (Pearce et al., 1992; Fig. 3). The concentration of zirconium normally increases in response to magmatic processes such as fractional crystallisation, excepted in the most differentiated lavas in which zircon has fractionated. SiO_2 vs. Zr (Fig. 3A) and TiO_2 vs. Zr (Fig. 3B) plots show that: (i) there exists

different SiO_2 values for similar Zr and TiO_2 contents, and (ii) the rocks cluster into three groups with limited overlap. Group 1 has low Zr, very low TiO_2 and high SiO_2 contents, group 2 has high Zr, relatively high TiO_2 and intermediate SiO_2 contents, and group 3 has transitional Zr, TiO_2 and low to relatively high SiO_2. The differences between the three groups reflect magmatic processes rather than alteration process, because both Ti and Zr are generally assumed to be relatively immobile during alteration and weathering.

Sr does not correlate with Zr (Fig. 3C) but most of the analysed samples cluster into two groups defined by low to transitional (50–180 ppm) and high (250–340 ppm) Zr contents at similar ranges of Sr. Part of the scattering of Sr data may be due to Sr mobility and/or plagioclase fractional crystallisation processes. Plagioclase fractionation is petrographically shown by tiled porphyritic intersertal textures in andesitic lavas. Further, plagioclase shows a high partition coefficient for Sr and Al, which appear to be correlated (the correlation coefficient, R^2, is of ~ 0.8 in most series). The Nd and Th vs. Zr plots (Fig. 3D–E) illustrate a positive correlation though scattering exceeds the uncertainty range of measurements for some samples. In order to investigate the relative mobility of Pb and U with respect to Th, the Ladakh lavas have been plotted in U and Pb vs. Th diagrams (Fig. 3F–G). The lavas display a linear trend in the U–Th plot suggesting that U was not mobilised relative to Th. In the Pb vs. Th diagram, the lavas are highly scattered but some samples of the Southern Group and the Eastern Ladakh lavas define two trends (1 and 2 in Fig. 3G).

These observations show the following.

(i) Sr and Pb could have been mobilised during the alteration and metamorphism experienced by Ladakh lavas.

(ii) Nd shows less variation, which indicate that alteration processes may have less affected Nd isotopic ratios. Considering the scale of sampling (N-Ladakh, 250×100 km), and duration of volcanism (20 Ma), its variations could be ascribed to magmatic processes rather than alteration.

(iii) Some samples (L58, L117, L118, L413 and LK9b) have been more intensely affected by alteration processes than the other studied lavas, spreading frequently out of the trends or fields.

In order to analyse the effects of alteration on the geochemical features of Ladakh samples, and particularly concerning their isotopic ratios, two of these latter volcanic rocks (L117 and L118) are compared to an unaltered sample (L116). L117 and L118 have been sampled in a zone of silicification and sulphur (pyrite, chalcopyrite) impregnation, in a fracture zone crosscutting the Southern Group of Western Ladakh (Fig. 1B). L117, sampled in the core of a 1–10-m thick silicification zone is a fine-grained recrystallised aphyric quartz–albite rock, characterised by a very high silica content (72.8 wt.%; Table 2). L118, sampled 10 m away from the visible silicification zone, shows also a fine-grained recrystallised matrix composed of quartz and epidote with quartz- and calcite-filled vesicles. Its high silica content (63.3 wt.%) suggests that silicification remains important outside of the visible zone of alteration. L116, sampled at approximately 100 m from the zone, shows a primary intersertal structure, with epidotised plagioclase, amphibolitised pyroxene and a chloritised glassy matrix, typical of greenschist grade metamorphism occurring in the rest of the series. Its silica content (55.5 wt.%) is close to the mean of the series (54 wt.%). Hydrothermal alteration is also evidenced by anomalous major element contents of samples L117 and L118 with respect to the other silica-rich lavas found in Eastern Ladakh (Fig. 4). L117 displays a particularly high Na_2O content (6.2 wt.%), while L118 is depleted in K, Na, Al, Mg and enriched in Ca and Ti. In Fig. 5, the trace element contents of L117 and L118 are compared to those of unaltered L116. Relative to L116 sample, L117 is depleted in most High Field Strength (HFS) elements except marked Nb, Ta, Zr and Hf enrichments, and shows paradoxical depletions in LREE and enrichments in LILE (Fig. 5A,B). These relative depletions are difficult to explain through differentiation processes, as depletion in LREE rarely correlates with silica enrichment. Preferential depletion of the most mobile LREE, and immobility of the most compatible HREE (Yb and Lu), could be explained by corrosive hydrothermal fluid alteration. Hydrothermal recrystallisation of albite can explain the relative enrichment in LILE, for which it has high partition coefficients, increasing with silica enrichment (Sr: 15.6; Rb: 0.11; Ba: 1.5; values for rhyolites in Nash and Crecraft, 1985). The Nb, Ta,

Table 2
Major and trace element analysis of most representative Ladakh volcanic rocks. Oxide values are normalised to 100% on anhydrous basis. Samples L199, L156, L174, L157, L116, L124, L118, L59, L175, L179, L573, L575 and LK 15 are representative analyses from Rolland et al. (2000), presented for comparison with complementary analyses from this study

Area	Western Ladakh												
Sample	L199	L156	L174	L157	L173	L116	L124	L118	L117	L55	L59	L65	L144
Type	A basalt	A basalt	A basalt	Andesite	Basalt	Andesite	Mg-rich	H L	H L	Nb–TiB	TD	AD	HMS
Unit	NG	NG	NG	NG	SG	SG	SG	SG	SG	SG	SG	SG	SG
Locality	Skoro lungma	Bauma Harel	Bauma Harel	Bauma Harel	Bauma Harel	Kussomik				Muchilu	Muchilu	Muchilu	Thalle pass
(wt.%)													
SiO_2	54.58	52.54	52.47	59.22	51.61	55.50	52.55	63.27	72.79	48.61	71.27	59.94	51.40
TiO_2	0.99	0.82	1.26	0.46	0.59	1.40	0.75	1.13	0.52	1.60	0.41	1.06	0.89
Al_2O_3	12.23	14.19	16.74	14.58	19.89	16.19	18.53	14.13	15.54	16.61	12.57	17.39	13.86
Fe_2O_3	1.73	1.81	1.63	1.18	1.51	1.81	1.53	1.14	0.19	1.93	0.99	0.95	1.56
FeO	8.80	9.24	8.31	6.01	7.70	9.26	7.83	5.82	0.96	9.86	5.06	4.86	7.94
MnO	0.16	0.16	0.18	0.13	0.17	0.23	0.51	0.19	0.03	0.21	0.11	0.09	0.17
MgO	8.43	8.23	7.02	7.06	4.94	3.23	9.59	0.47	1.38	6.44	2.17	2.50	9.81
CaO	9.62	7.57	8.00	7.11	9.89	8.77	7.91	13.14	1.29	12.22	3.69	5.52	8.62
Na_2O	2.65	4.96	4.21	4.06	2.63	2.16	0.54	0.24	6.20	2.06	3.22	4.31	1.98
K_2O	0.72	0.41	0.08	0.13	0.98	1.01	0.11	0.08	1.05	0.13	0.41	2.76	3.31
P_2O_5	0.08	0.07	0.10	0.05	0.11	0.44	0.16	0.39	0.04	0.33	0.08	0.62	0.46
LOI	2.70	1.04	2.17	2.01	4.14	0.93	5.23	1.39	0.60	2.71	2.78	0.58	2.69
(ppm)													
Ba	5	28	20	20	147	111	10	9	135	60	44	759	500
Rb	10.12	8.32	0.89	0.69	18.64	20.89	2.17	2.19	26.08	2.78	5.63	62.28	60.02
Sr	111	262	128	115	441	481	219	954	202	451	238	1132	453
Ta	0.18	0.31	0.12	0.04	0.06	0.46	0.17	0.39	0.92	1.28	0.05	0.77	0.24
Th	0.32	0.31	0.08	0.17	0.70	2.23	0.96	1.60	3.17	1.09	0.23	6.37	2.18
Zr	60	55	89	44	44	149	70	116	286	126	43	308	72
Nb	2.6	4.5	1.4	0.4	0.9	7.0	2.8	4.7	14.1	15.8	0.6	17.5	3.8
Y	26.29	16.87	31.16	11.87	15.27	49.94	17.16	35.08	30.83	27.94	15.85	15.51	16.48
Hf	0.90	0.89	1.16	0.69	0.51	3.74	1.36	2.17	2.24	0.80	0.45	5.81	2.11
Co	129.45	56.41	33.43	40.67	34.68	58.53	78.36	58.98	40.43	193.06	35.18	26.51	45.11
U	0.30	0.07	0.06	0.08	0.22	0.76	0.34	0.51	0.61	0.38	0.47	1.94	0.74
Pb	0.29	0.97	–	0.33	2.47	5.92	2.93	5.59	1.86	8.89	2.49	15.35	5.94
Cs	0.29	4.55	0.22	0.19	1.01	0.53	0.11	0.09	0.69	0.02	0.75	2.10	1.37
La	3.57	3.46	2.21	1.34	5.36	15.40	6.58	11.08	2.61	13.07	2.56	49.09	14.53
Ce	8.70	7.67	7.72	3.61	11.38	37.98	14.97	27.04	6.58	30.61	5.54	98.66	32.21
Pr	1.32	1.07	1.40	0.59	1.58	5.48	2.06	3.90	0.97	3.98	0.89	11.29	4.34
Nd	6.60	4.99	7.61	3.21	7.09	26.24	9.48	18.85	4.82	17.40	4.61	41.17	18.57
Sm	2.34	1.64	2.77	1.09	1.84	7.21	2.61	5.24	1.74	4.30	1.54	6.62	4.20
Eu	1.08	0.59	1.03	0.45	0.65	2.07	0.73	1.54	0.69	1.43	0.51	1.74	1.27
Gd	2.83	2.39	3.80	1.53	2.0629	7.16	2.54	5.15	2.33	4.23	1.73	5.15	4.09
Tb	0.58	0.48	0.74	0.28	0.36	1.30	0.46	0.94	0.54	0.68	0.35	2.48	0.54
Dy	4.18	3.34	4.97	1.85	2.30	7.51	2.67	5.36	3.85	4.02	2.24	0.43	2.93
Ho	1.00	0.76	1.09	0.40	0.52	1.58	0.55	1.11	0.91	0.86	0.50	1.07	0.58
Er	2.61	2.19	2.97	1.14	1.46	4.75	1.61	3.24	2.92	2.16	1.53	0.15	1.58
Yb	2.35	2.17	2.58	1.11	1.37	4.38	1.46	2.90	2.98	1.92	1.44	0.83	1.42
Lu	0.34	0.34	0.37	0.17	0.20	0.66	0.23	0.43	0.43	0.30	0.21	0.12	0.22

NG: Northern Group; SG: Southern Group; KF: Katzarah Formation; H L: hydrothermalised lava; TD: tholeiitic dacite; A basalt: Andesitic basalt; Nb–TiB: High Nb–Ti basalt.

				Eastern Ladakh								
L175	L179	L573	L575	L318	L424	L317	L320	L344	LK 15	L399	BHVO certifiate standard errors (%)	
Nb–TiB KF Shigar	Nb–TiB KF Shigar	Nb–TiB KF Katchoura	Nb–TiB KF	Basalt Teah	Basalt Tangyaar	Andesite Teah	Andesite Teah	Dacite Deskhit	Rhyolite Deskhit	(diorite) Chang la		
50.97	50.36	48.96	53.91	51.56	51.84	57.91	61.94	68.52	79.10	–	–	
2.07	2.49	0.83	0.77	1.05	1.73	1.66	0.84	0.53	0.12	–	2.75	1.2
12.21	16.93	15.47	12.30	17.98	21.34	14.98	17.91	13.90	11.37	–	13.53	0.7
1.68	1.86	1.26	1.09	1.56	1.44	1.76	1.00	1.00	0.16	–	11.23	1.0
8.59	9.49	6.41	5.57	7.95	7.36	8.97	5.11	5.12	0.81	–	0.17	0.7
0.17	0.19	0.26	0.12	0.22	0.15	0.20	0.18	0.07	0.12	–	7.23	0.9
11.79	5.63	9.05	13.16	6.10	3.22	3.38	3.92	2.77	0.10	–	11.01	0.8
9.28	8.58	15.90	11.50	10.66	7.72	5.86	2.82	3.46	1.02	–	2.22	1.9
2.73	3.49	1.35	1.11	2.37	3.24	2.79	4.74	4.04	3.27	–	1.09	1.6
0.27	0.75	0.52	0.35	0.34	1.95	2.03	1.45	0.54	3.91	–	0.23	3.3
0.24	0.24	–	0.12	0.19	0.01	0.45	0.08	0.05	0.02	–	mean ($n = 9$) (ppm)	standard deviation (%)
2.94	2.57	3.55	1.12	0.75	2.03	0.29	1.44	1.64	1.32			
139	69	116	72	66	401	339	313	289	506	331	132.47	3.7
3.97	5.76	10.30	7.22	12.35	94.31	76.80	39.04	6.66	122.84	172.26	9.08	0.3
219	163	249	200	417	430	265	349	182	104	66	402.67	10
1.23	0.80	1.17	0.60	0.17	0.88	0.71	0.47	0.11	0.81	0.56	1.25	0.1
1.75	0.94	1.83	0.79	1.25	9.37	9.49	6.38	1.11	14.25	8.18	1.10	0.02
145	164	39	54	62	310	241	118	22	82	78	186.63	5.8
18.7	12.0	18.5	9.1	2.7	13.7	10.1	6.3	1.8	10.1	7.5	20.32	1.0
19.84	31.10	16.42	13.65	20.28	52.24	47.79	21.31	11.46	26.40	30.47	27.31	0.7
1.54	1.17	1.12	1.39	1.68	7.44	6.39	3.13	0.79	2.88	2.17	4.54	0.2
49.75	36.16	43.16	56.71	40.71	28.08	30.92	22.71	17.13	1.25	39.65	44.95	0.6
0.34	0.25	0.31	0.26	0.33	2.29	1.85	1.37	0.44	2.12	0.92	0.41	0.01
2.27	1.00	1.06	1.09	7.17	8.20	18.32	13.81	1.11	13.51	11.77	2.07	0.2
0.62	0.25	0.57	0.68	5.40	5.60	6.84	4.60	0.51	4.35	21.91	0.10	0.01
15.73	11.76	11.71	7.20	7.96	33.17	31.58	14.78	3.86	19.40	21.86	15.84	0.4
37.54	29.40	21.28	15.62	19.11	75.45	71.99	34.79	8.49	42.94	39.62	38.22	0.9
4.87	4.15	2.49	1.99	2.59	9.56	9.17	3.89	1.08	4.65	4.91	5.44	0.1
20.55	19.06	9.70	8.45	11.47	39.39	37.49	15.24	4.60	16.89	18.81	24.89	0.4
4.76	5.20	2.11	2.02	2.90	8.97	8.45	3.45	1.26	3.77	4.01	6.14	0.1
1.43	1.77	0.70	0.70	1.04	2.13	1.97	0.91	0.41	0.61	0.87	2.02	0.05
4.62	5.715	2.314	2.27	3.39	9.34	8.79	3.53	1.59	3.96	4.32	6.28	0.2
0.72	0.99	0.38	0.37	0.55	1.40	1.31	0.55	0.26	0.61	0.70	0.95	0.02
4.02	5.96	2.43	2.27	3.39	8.42	8.14	3.39	1.72	3.44	4.30	5.38	0.1
0.74	1.17	0.52	0.48	0.72	1.81	1.66	0.71	0.38	0.74	0.92	1.01	0.03
1.78	3.02	1.43	1.33	2.03	4.86	4.70	2.04	1.14	2.41	2.52	2.42	0.06
1.24	2.17	1.54	1.21	1.79	4.43	4.20	2.04	1.15	2.76	2.83	2.02	0.05
0.15	0.27	0.24	0.18	0.28	0.70	0.64	0.32	0.19	0.45	0.45	0.29	0.01

Table 3
Sr, Nd and Pb isotopic data of Western and Eastern Ladakh areas. Isotopic ratios have been corrected from in situ decay assuming an age of 110 Ma

Sample no.	Type		$^{143}Nd/^{144}Nd$	$\pm(2\sigma)$	$^{87}Sr/^{86}Sr^{*}$	$\pm(2\ s)$	$^{147}Sm/^{144}Nd$	$(^{143}Nd/^{144}Nd)_{110}$
Western Ladakh								
L140	Back-arc	Type 1	0.512838	±12	0.704352	±7	0.189885	0.512702
L156	Back-arc	Type 1	0.512976	±7	0.705492	±17	0.199071	0.512833
L174	Back-arc	Type 2	0.513059	±5	0.705059	±9	0.219181	0.512901
L157	Back-arc	Type 2	0.512989	±2	0.704378	±9	0.205179	0.512842
L116	BA	Kussomik	0.512901	±7	0.704123	±12	0.166145	0.512781
L118	Hydro. B	Kussomik	0.512918	±9	0.704312	±14	0.160883	0.512802
L117	Hydro. B	Kussomik	0.512985	±5	0.704878	±10	0.200478	0.512841
L144	HMS	Thalle Pass	0.512829	±7	0.704686	±11	0.136559	0.512730
L59	TD	Muchilu	0.512895	±14	0.705454	±10	0.201580	0.512750
L65	AD	Muchilu	0.512653	±4.5	0.704859	±11	0.097848	0.512583
L55	High Nb–Ti	Muchilu	0.512514	±6	0.709355	±9	0.149398	0.512406
L55	High Nb–Ti	(duplicate)	0.512500	±5	–	–	0.149398	0.512392
L175	High Nb–Ti	Shigar	0.512726	±3	–	–	0.139978	0.512616
L179	High Nb–Ti	Shigar	0.512790	±5	–	–	0.164944	0.512660
L573	High Nb–Ti	Katchoura	0.512828	±7	–	–	0.131624	0.512725
L575	High Nb–Ti	Katchoura	0.512827	±7	–	–	0.144317	0.512713
Eastern Ladakh								
L318	basalt	Teah	0.5127594*	±4	–	–	0.153015	0.512639
L317	andesite	Teah	0.5127289*	±5	–	–	0.136249	0.512622
L424	basalt	Deskhit	0.5128774**	±7	–	–	0.137675	0.512778
L352	andesite	Deskhit	0.5127575*	±8	0.704460	±10	0.138714	0.512658
L352	pyroxene	Deskhit	–	–	–	–	–	–
L356	andesite	Deskhit	0.5127451*	±7	–	–	0.138699	0.512636
L423	andesite	Deskhit	0.5126865**	±10	–	–	0.135155	0.512589
L344	dacite	Deskhit	0.5126371*	±6	–	–	0.157548	0.512513
LK96b	Dacite	Deskhit	0.5127936*	±5	–	–	0.131581	0.512690
LK16	rhyolite	Deskhit	0.5126759*	±6	–	–	0.110220	0.512589
L397	gabbro	Chang La	0.51313**	±11	–	–	0.280853	0.512928
L399	diorite	Chang La	0.5122056**	±10	–	–	0.280792	0.512004

*: analyses obtained a University P. Sabatier of Toulouse; **: analyses obtained at ENS Lyon; BA: basaltic andesite; Hydro. B: hydrothermalised basalt; HMS: High-Mg shoshonite; TD: tholeiitic dacite; AD: adakite.

Zr and Hf enrichments (with anomalous Zr/Hf ratio of 128) can be either due to the presence of zircon, petrographically observed in L117, and other minerals unaffected by alteration, or to a volume decrease due to depletions of most major elements (and thus relative enrichments of immobile elements). In contrast, L118 shows quite similar trace element contents as L116 and the rest of Southern Group lavas (see Section 4.2.2), with the exception of the most mobile LILE (Fig. 5A). This depletion in LILE can be due to absence of albite recrystallisation and substitution of plagioclase by calcite and epidote, as the lava was in the periphery of the main hydrothermal zone.

In order to check whether hydrothermal alteration has had any effects on the Nd, Sr and Pb isotopic compositions, samples L116, L117 and L118 have been analysed (Table 3). The εNd ratio of the most hydrothermalised sample (L117) is higher (+6.7) than those of samples L116 and L118 (+5.96 and +5.56, respectively). The $(^{87}Sr/^{86}Sr)_{110\ Ma}$ of the two altered basalts (L117 and L118) are significantly higher than the preserved one (L116). The Pb isotopic ratios of L117 are also slightly higher than those of L116.

From this section, hydrothermal alteration is shown to have an effect on relatively localised zones (~ 100 m), element mobility decreasing rapidly from

$\varepsilon(Nd)_{110}$	$^{87}Rb/^{86}Sr$	$(^{87}Sr/^{86}Sr)_{110}$	$\varepsilon(Sr)_{110}$	$^{208}Pb/^{204}Pb^{**}$	$^{207}Pb/^{204}Pb^{**}$	$^{206}Pb/^{204}Pb^{**}$	$\Delta 7/4$	$\Delta 8/4$
4.01	0.75	0.719627	−0.73	–	–	–	–	–
6.57	0.09	0.705348	13.88	–	–	–	–	–
7.89	0.02	0.705028	9.33	38.664	15.571	18.407	8.51	78.36
6.74	0.02	0.704351	−0.28	38.797	15.589	18.693	7.16	57.02
5.56	0.13	0.703927	−6.31	38.374	15.551	18.361	6.95	54.86
5.96	0.01	0.704299	−1.02	–	–	–	–	–
6.72	0.27	0.704450	1.12	38.666	15.612	18.549	11.04	61.34
4.56	0.38	0.704087	−4.03	38.640	15.544	18.589	3.81	53.89
4.94	0.07	0.705347	13.85	–	–	–	–	–
1.68	1.62	0.702324	−29.05	39.004	15.669	18.569	15.35	79.65
−1.76	0.02	0.709327	70.36	39.072	15.694	18.569	18.98	99.45
−2.03	–	–	–	–	–	–	–	–
2.59	–	–	–	39.311	15.600	19.000	4.99	71.36
3.44	–	–	–	39.509	15.624	19.262	4.50	59.37
4.70	–	–	–	38.554	15.527	18.216	6.18	90.45
4.48	–	–	–	38.305	15.506	18.142	4.84	74.43
3.04	–	–	–	38.705	15.607	18.520	10.82	68.70
2.70	–	–	–	38.846	15.623	18.594	11.65	73.92
5.50	–	–	–	–	–	–	–	–
3.15	0.16	0.70421	−2.26	38.662	15.578	18.510	8.07	65.60
–	–	–	–	38.763	15.603	18.569	9.87	68.61
2.98	–	–	–	–	–	–	–	–
1.81	–	–	–	38.750	15.621	18.523	12.22	72.93
0.58	–	–	–	39.223	15.627	19.102	6.54	50.22
4.03	–	–	–	–	–	–	–	–
2.06	–	–	–	–	–	–	–	–
8.42	–	–	–	–	–	–	–	–
−9.62	–	–	–	–	–	–	–	–

the main fluid circulation zones. Data shows a decoupling of major vs. trace elements, and also of LILE vs. HFSE, which could be due to diffuse and unpredictable element mobility. Consequently, to reduce problems of misinterpretation linked to alteration effects, only most representative samples showing a lesser degree of major and trace element variation from the differentiation trend of the series have been selected for isotopic analyses.

4.2.2. Major and trace element, and Sr, Nd, Pb isotopic compositions of Ladakh units

Main geochemical differences between the geological units defined from field study are summarised below. They are deduced from major and trace element data presented in Rolland et al. (2000) and complementary data from this paper.

4.2.2.1. Northern group mafic lavas: back-arc basin affinity. The Northern Group pillow-lavas (four samples in Table 2) exhibit high FeO_t and MgO, and low CaO, Al_2O_3 and TiO_2 contents. Northern Group lavas show trace and REE contents close to those of N-MORB (Fig. 6A). Two types have been distinguished on the basis of trace elements and REE contents. Type 1 is slightly enriched in LREE [e.g. $(La/Sm)_N$ and $(La/Yb)_N$ in Table 4], with LILE and Th enrichments [e.g. high $(Th/Yb)_N$ in Table

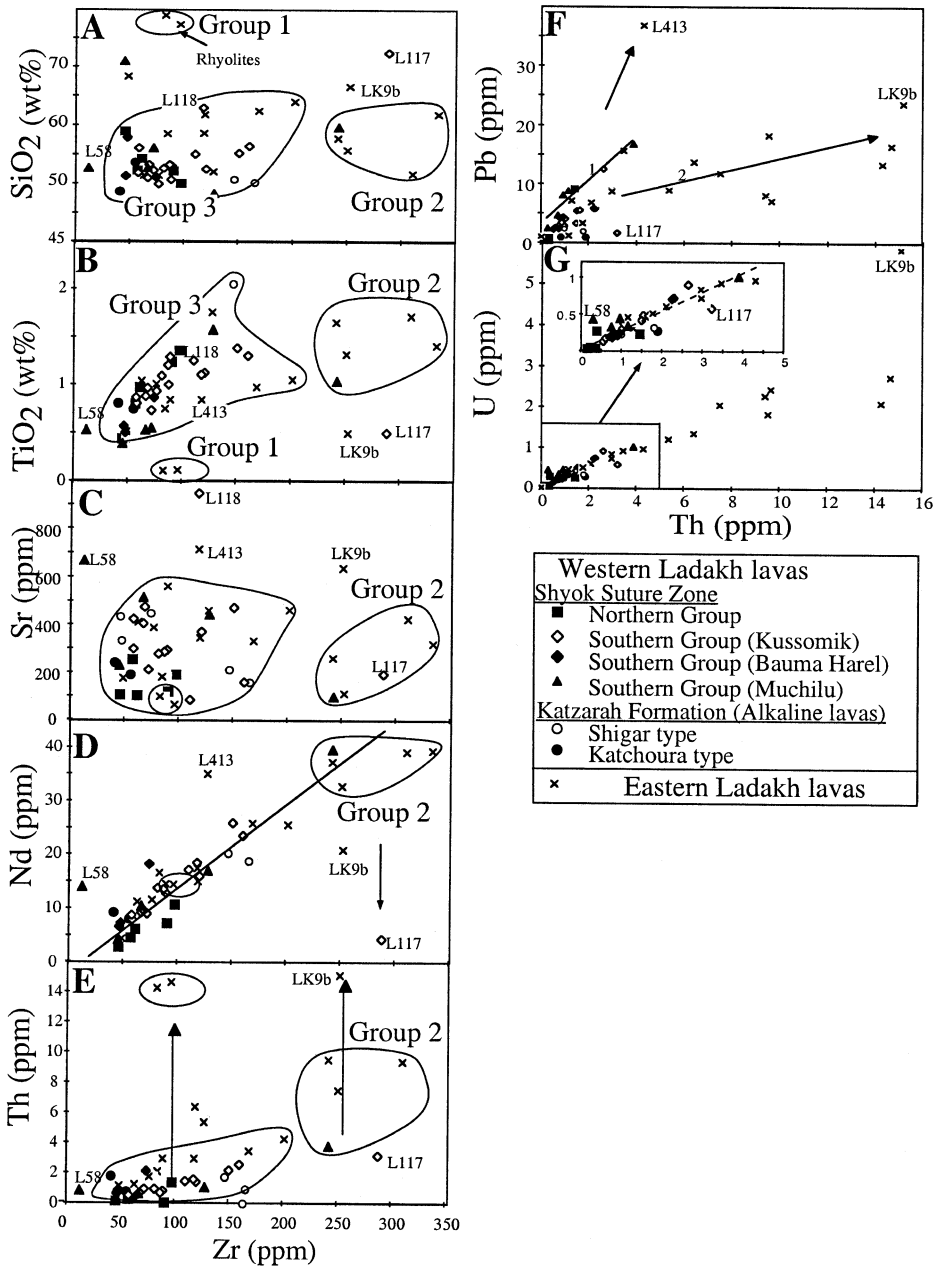

Fig. 3. Major and trace elements vs. Zr and Th diagrams. Major and trace elements are chosen to investigate the effects of alteration on the Sr, Nd and Pb isotopic systems. Groups 1–3: see explanations in the text.

4], relative to chondritic and MORB values. Type 2 is LREE-depleted ($(La/Sm)_N$ and $(La/Yb)_N$ are less than 1), and does not show the Th and LILE enrichments of Type 1 [low $(Th/Yb)_N$; Table 4]. Northern Group lavas have high and rather homogeneous εNd_{110}, with the exception of Type 1 basalt L140 that has a significantly lower εNd_{110} (Table 3; Fig. 7A). The εSr_{110} ratios span a large range of

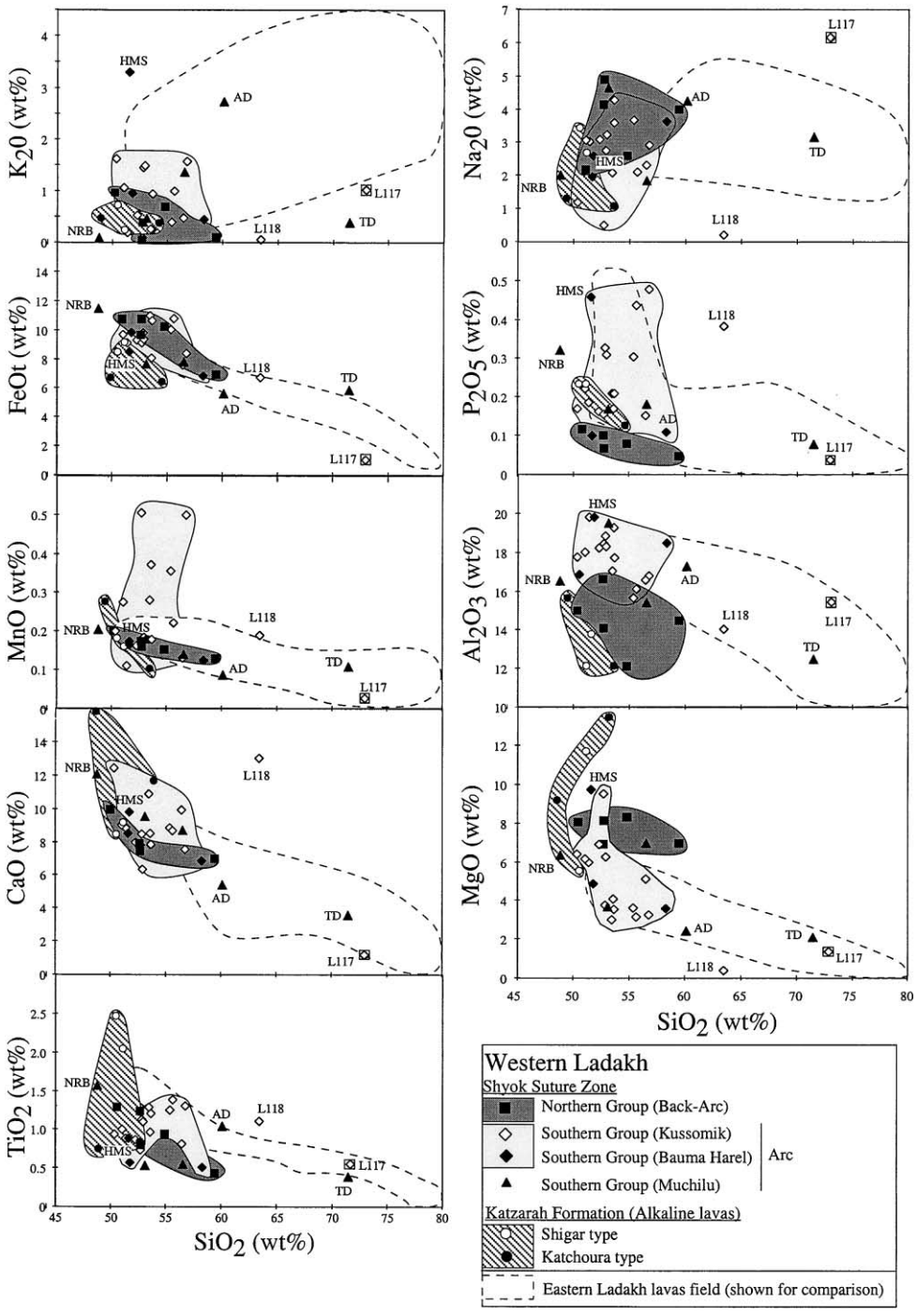

Fig. 4. Harker variation diagrams of Western Ladakh volcanic rocks. Eastern Ladakh lavas field is shown for comparison. AD: adakitic lava, HMS: high-Mg shoshonitic basalt, NRB: Nb-rich basalt, TD: Tholeiitic Dacite.

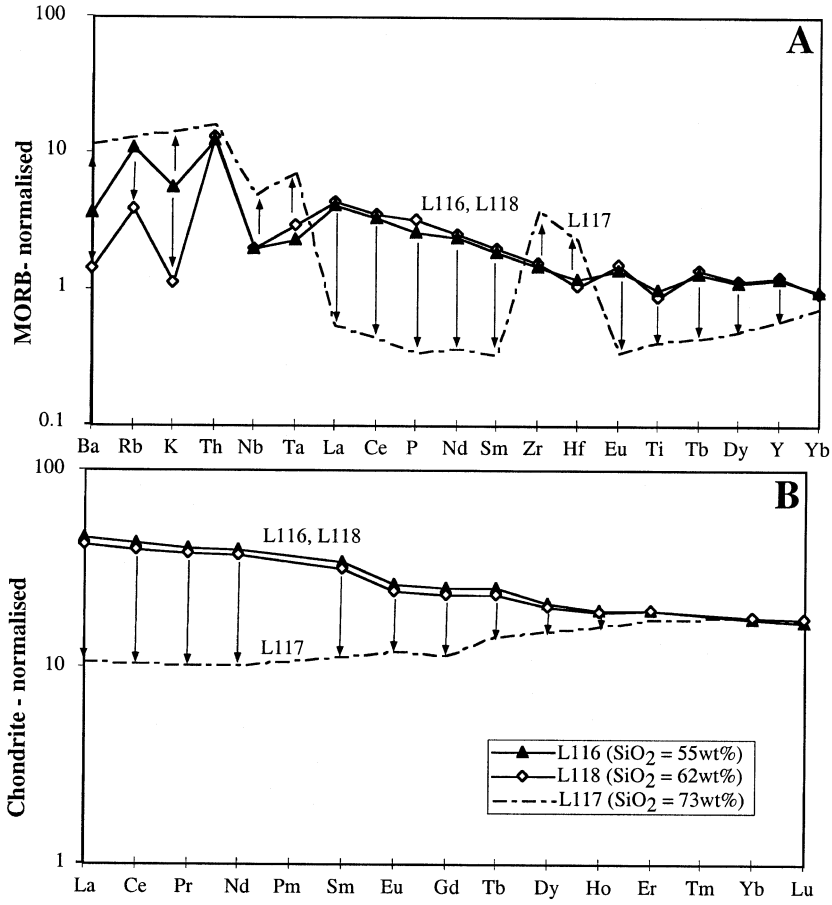

Fig. 5. (A) Major and trace elements spidergrams, and (B) REE patterns, of hydrothermalised samples. L117 was sampled in the core of the zone of hydrothermal silicification, while L118 was sampled 10 m from the core of the hydrothermal zone and L116 has been collected at ~ 100 m from the zone. Chondritic normalisation values are those of Evensen et al., 1978 and MORB normalisation values are those of Sun and MacDonough (1989). Note the depletion in LREE and MREE and the relative enrichment in Nb, Ta, Zr, Hf and LILE of the most hydrothermalised sample (L117).

values (from -0.78 to $+13.88$) which do not correlate with the εNd_{110}. Pb isotopic ratios are in the same range as the arc-related Southern Group (described below), with $38.664 < {}^{208}Pb/{}^{204}Pb < 38.797$, $15.571 < {}^{207}Pb/{}^{204}Pb < 15.589$ and $18.407 < {}^{206}Pb/{}^{204}Pb < 18.693$ (Table 3).

Considering major and trace elements and REE, Northern Group lavas show tholeiitic affinities, transitional between N-MORB and Island arc tholeiites (IAT). Northern Group lavas have higher εNd_{110} than the rest of the analysed Ladakh lavas, indicating a more Nd-depleted source. Considering both the sedimentary environment dominated by avalanche-type deposits featuring a marginal basin, and the geochemistry, the Northern Group could be interpreted as the remnant of back-arc basin series developed on the northern side of the arc.

4.2.2.2. Southern group lavas: intra-oceanic arc tholeiitic affinity. Most of the Southern Group lavas (Kussomik suite in the Upper Thalle Valley, Muchilu and Bauma Harel, Fig. 1B) occur as pillowed or massive flows and tuffs. The lavas are basaltic andesites in composition, with high Al_2O_3 and low TiO_2 (0.7–1.4 wt.%) contents. Moreover, they are Th and LILE enriched, and display strong Nb and Ta depletions [e.g. low $(Nb/La)_N$ for the Kussomik suite, and very low $(Nb/La)_N$ for the lavas from

Table 4
Summarised geochemical features of Western and Eastern Ladakh units
Values are in wt.%.

Area	Western Ladakh						Eastern Ladakh	
Units	Northern Group		Southern Group		Katzarah Formation			
					Katchoura type	Shigar type		
SiO_2	50–59		52–56		49–54	50–51	52–79	
FeO_t	7–11		8–12		6–7	9–10	10–11[a]	
MgO	7–8		3.0–9.6		9.1–13.2	5.6–11.8	3.2–6.1[a]	
Na_2O	2.2–5		0.5–4.7		1.1–1.4	1.1–1.4	2.2–3.2[a]	
CaO	7.1–10.7		6.4–9.9		11–15	11.5–16	7.7–10.7[a]	
Al_2O_3	12.2–16.7		16.2–19.9		12.3–15.5	12.3–15.5	18.0–21.3[a]	
K_2O	0.08–1.02		0.3–1.7		0.3–0.5	0.4–0.5	0.2–2.0[a]	
TiO_2	0.46–1.36		0.6–1.4		0.8	2.0–2.5	1.1–1.7[a]	
	Type1	Type 2	Kussomik suite	Muchilu-Bauma Harel				
$(La/Sm)_N$	1.0–1.3	0.5–0.8	1.0–1.6	1.8–3.0	1.4–2.8	2.2–3.5	1.8–2.4[b]	3.2–6.5[c]
$(La/Yb)_N$	1.0–1.4	0.6–0.8	1.8–3.0	2.6–3.9	3.4–3.5	4.4–9.8	2.5–5.7[b]	6.8–13.0[c]
$(Th/Yb)_N$	3.5–11.5	0.8–3.9	7–22	12–15	13–15	11–36	18–56[b]	131–251[c]
$(Nb/La)_N$	0.3–0.7	0.7–1.4	0.3–0.6	0.1–0.2	1.4–1.7	1.4–2.1	0.4–0.5[b]	0.4–0.6[c]
$^{143}Nd/^{144}Nd$	0.5127–0.5128	0.5128–0.5129	0.5127–0.5128	–	0.5127	0.5126–0.5127	0.5126–0.5128[b]	0.5125–0.5127[c]
εNd_{110}	+4–+7	+7–+8	+5–+6	–	+4–+5	+3	(+1.8–+5.52)[b]	(+0.5–+4)[c]
$^{87}Sr/^{86}Sr$	0.7044–0.7196	0.7044–0.7050	0.7039–0.7045	–	–	–	0.7042[b]	–
εSr_{110}	−0.7–+14	0–+9	−6–−1	–	–	–	(−2)[b]	–
$^{206}Pb/^{204}Pb$	–	18.41–18.69	18.36–18.59	–	18.14–18.22	19.00–19.26	18.52–19.10[b]	19.10[c]
$^{207}Pb/^{204}Pb$	–	15.57–15.59	15.54–15.61	–	15.51–15.53	15.60–15.62	15.60–15.62[b]	15.63[c]
$^{208}Pb/^{204}Pb$	–	38.66–38.80	38.40–38.70	–	38.31–38.6	39.31–39.51	38.70–38.80[b]	39.22[c]

[a] Values for basalts.
[b] Values for basalts to andesites.
[c] Values for dacites to rhyolites.

Muchilu and Upper Bauma Harel; Fig. 6B–D; Table 4]. All lavas of the Southern Group show LREE enrichment. The lavas of the Muchilu and Bauma Harel suites display higher LREE enrichments than those of Kussomik suite [e.g. $(La/Sm)_N$ and $(La/Yb)_N$ ratios in Table 4]. Relatively to the Northern Group lavas, Southern Group lavas show slightly lower εNd_{110} and εSr_{110} values, and similar Pb isotopic ratios (Tables 3 and 4; Fig. 7A).

Considering the geological context, lithologies being exclusively volcanic, and the geochemical data, the Southern Group features a tholeiitic intra-oceanic volcanic arc environment.

4.2.2.3. Particular lava types of the Western Ladakh Southern Group. Among the lavas of the Southern Group, four samples, viz. (i) a tholeiitic dacite, (ii) a Mg-rich shoshonitic basalt, (iii) a Nb-rich basalt, and (iv) an adakitic lava, differ from the arc-tholeiites by distinct major, trace and isotopic compositions. The tholeiitic dacite, the Nb-rich basalt and the adakitic lava were sampled near Muchilu while the Mg-rich shoshonitic basalt was collected near the Thalle Pass, all interlayered in the volcanic arc series (Fig. 1B).

Tholeiitic dacite. The dacite L59 ($SiO_2 = 71.27$ wt.%) differs from those from Eastern Ladakh by low K_2O (0.4 wt.%) and relatively high FeO_t (6.5

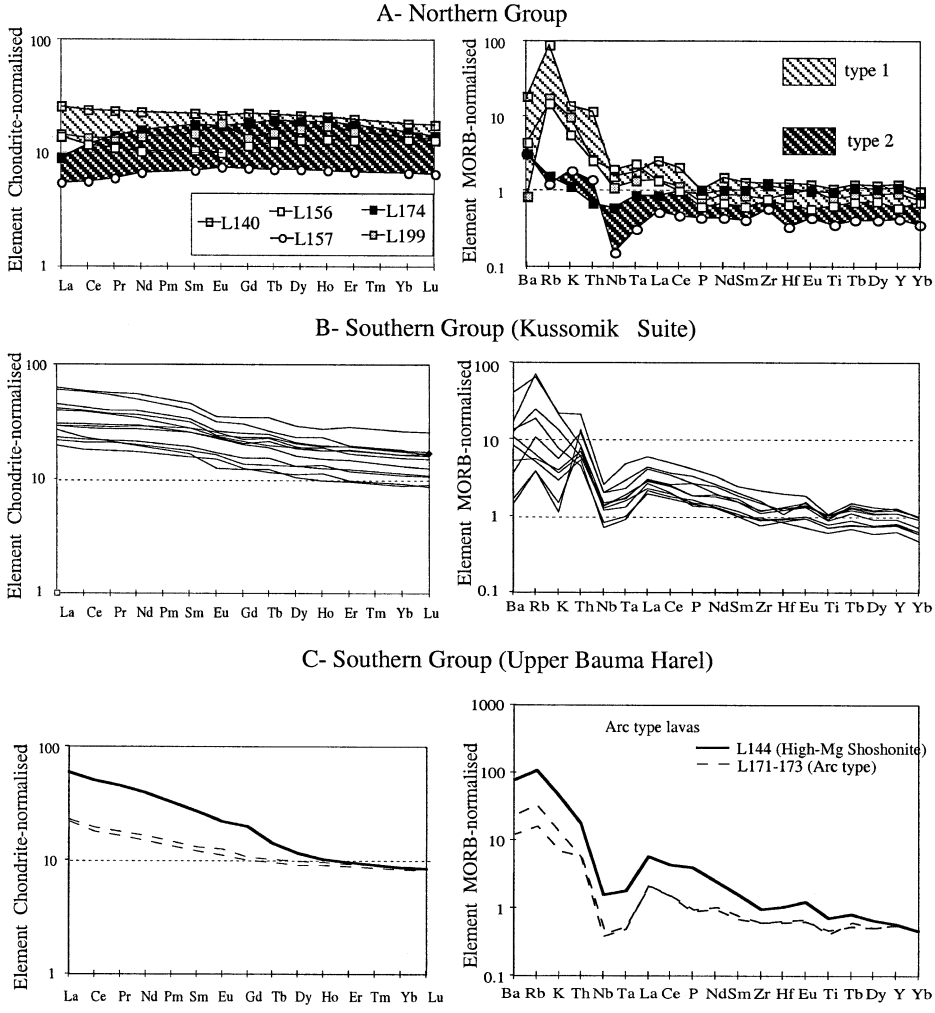

Fig. 6. REE and trace diagrams. Same normalisation values as in Fig. 5.

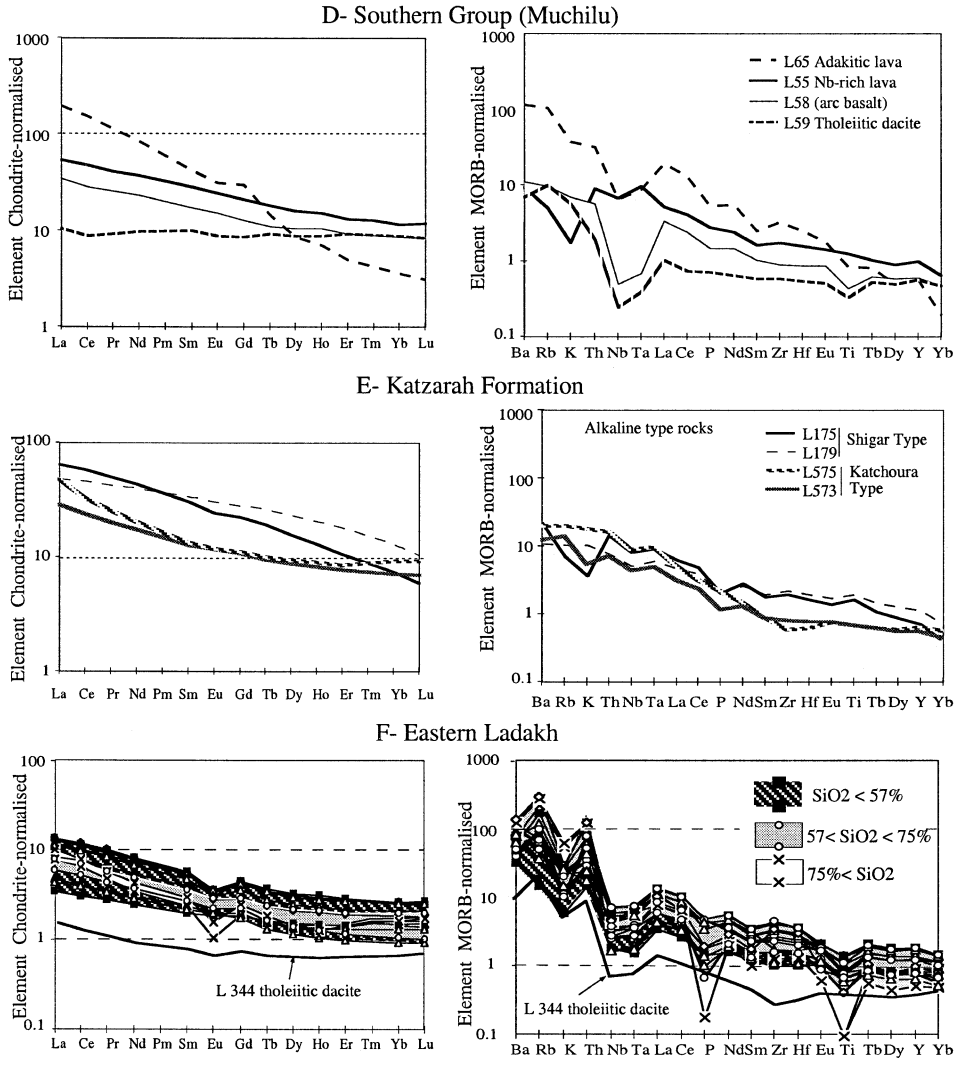

Fig. 6 (*continued*).

wt.%) contents. Its trace element contents are lower than in basalts and basaltic andesites of the Southern Group (Fig. 6D). Moreover, this tholeiitic dacite has a flat REE pattern, and strong Nb and Ta negative anomalies [relative to MORB; $(Nb/La)_N = 0.23$], which are characteristics of tholeiitic arc-lavas. Its εNd_{110} (+4.94) and εSr_{110} (+13.85) are lower than those of most Western Ladakh lavas (Fig. 7A; Table 3).

Mg-rich shoshonitic basalt. This basalt (L144) differs from the arc-tholeiites of the Southern Group by high K_2O (3.3 wt.%) and MgO (9.8 wt.%) contents. The MORB normalised multi-element plot of this basalt (Fig. 6C) shows high LILE (Ba = 500 ppm) and LREE enrichments [$(La/Sm)_N = 2.1$) correlated with a slight HREE depletion $(Yb)_N = 6.8$] and marked Nb and Ta negative anomalies [$(Nb/La)_N = 0.28$] relative to Southern Group arc lavas. Moreover, this basalt is characterised by a lower εNd_{110} than those of most Western Ladakh lavas (+4.56), similarly to the tholeiitic dacite. Its εSr_{110} is lower than that of the dacite (−4.03). Its

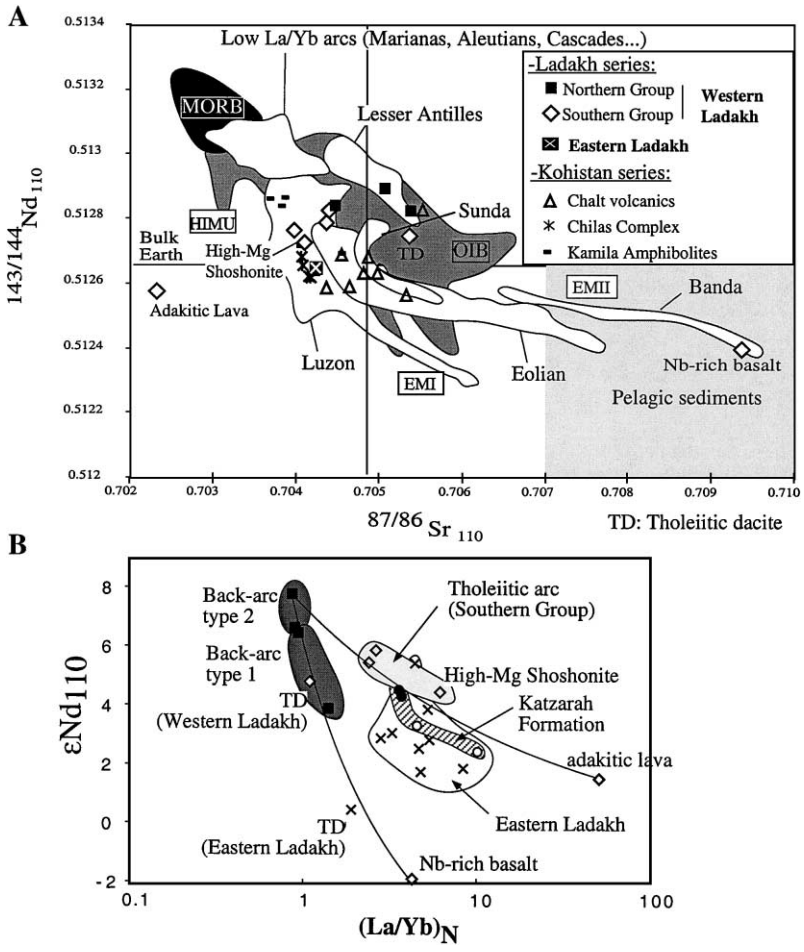

Fig. 7. (A) Isotopic $(^{143}Nd/^{144}Nd)_{110}$–$(^{87}Sr/^{86}Sr)_{110}$ plot. Values of Kohistan series are from Khan et al. (1997), recalculated to 110 Ma; values of oceanic arc are from Hawkesworth et al. (1994). (B) εNd_{110} vs. chondrite-normalised (La/Yb) diagram, showing the negative correlation of εNd with LREE enrichment. Note the εNd decrease and La/Yb increase from the Western Ladakh Northern Group lavas to the Eastern Ladakh lavas.

Pb isotopic ratios are lower than those of the arc-tholeiites and/or back-arc basin lavas ($^{208}Pb/^{204}Pb = 38.640$, $^{207}Pb/^{204}Pb = 15.544$ and $^{206}Pb/^{204}Pb = 18.589$; Fig. 7A and Table 3).

Nb-rich basalt. The major element abundances of basalt L55 are transitional between those of the Southern Group arc-tholeiites and the Katzarah Nb–Ti rich lavas (next section). Indeed, this basalt has higher TiO_2 (1.5 wt.%), FeO_t (11.6 wt.%) and CaO (12.2 wt.%) and lower Al_2O_3 (16.6 wt.%] contents than the Southern Group arc-tholeiites. L55 has high Nb, Ta $[(Nb/La)_N = 1.30]$, Th and LREE contents (Table 2), and do not display the Ti negative anomaly (Fig. 6D). L55 has particularly low εNd_{110} (−1.76; duplicate: −2.03), high εSr_{110} (+70.36) and high Pb isotopic ratios ($^{208}Pb/^{204}Pb = 39.072$, $^{207}Pb/^{204}Pb = 15.694$ and $^{206}Pb/^{204}Pb = 18.569$) which are far more radiogenic than those of any Ladakh lava (Fig. 7A).

Adakitic lava. The mineralogy and major elements compositions of this felsic lava (L65) are similar to adakites (Table 2; Fig. 4). L65 is composed of abundant plagioclase (An 20), and less abundant hornblende, biotite and sphene phenocrysts. On the basis of its major element composition ($SiO_2 = 59.9$ wt.%; $Na_2O = 4.31$ wt.%; $K_2O =$

2.8 wt.%), L65 is quite similar to Eastern Shyok andesites. L65 has high LILE contents, (Ba = 759 ppm), including a high Sr content (1132 ppm), a strong LREE enrichment ($(La/Sm)_N = 4.7$) and a marked HREE depletion ($(La/Yb)_N = 40$; Fig. 6D). The low HREE contents (Yb = 0.8 ppm) and high Sr/Y ratio (Sr/Y = 73) of sample L65 are similar to adakites (Martin, 1986, 1999). L65 displays also marked Nb and Ta negative anomalies ($(Nb/La)_N = 0.4$), which are common features for adakites. L65 shows lower εNd_{110} (+1.68) and high Pb isotopic ratios ($^{208}Pb/^{204}Pb = 39.004$, $^{207}Pb/^{204}Pb = 15.669$ and $^{206}Pb/^{204}Pb = 18.667$) similarly as L55 Nb-rich basalt (Table 3; Fig. 7A).

4.2.2.4. The Katzarah Formation. The lavas of the Katzarah Formation can be divided into two types on the basis of the major element contents and REE patterns (Fig. 6E and Table 2). The Katchoura type (Fig. 1B) is characterised by high CaO and MgO abundances and low FeO_t and TiO_2 contents. The Shigar type (Fig. 1B) differs from the Katchoura type by high TiO_2 and lower CaO contents (Table 4). Both types show low but variable Al_2O_3 contents. The two most Mg-rich samples (L575 and L175) of both Katchoura and Shigar types show picritic compositions with Mg# of 0.7 and 0.8, respectively. The Katchoura type lavas are flat-HREE patterned (Fig. 6E), while the Shigar type rocks have fractionated HREE.

Both lava types are LREE, LILE and Th enriched [e.g. $(Th/Yb)_N$; $(La/Sm)_N$ and $(La/Yb)_N$ ratios in Table 4] and are not depleted in Nb [$(Nb/La)_N \sim 1$], Ta and TiO_2. Katzarah lavas have lower εNd_{110} ratios than Northern and Southern group lavas. However, the Katchoura and Shigar types are isotopically distinct. The Katchoura type has higher εNd_{110} and lower $^{208}Pb/^{204}Pb$, $^{207}Pb/^{204}Pb$ and $^{206}Pb/^{204}Pb$ than the Shigar type (Tables 3 and 4). Considering major, trace and isotopic compositions, Katzarah Formation lavas have similar features to Oceanic Island Basalts (OIB).

4.2.2.5. Eastern Ladakh volcanic rocks. Eastern Ladakh samples were collected along the Shyok Suture Zone in northern Ladakh, north of the Ladakh Batholith (Nubra-Shyok area: Khardung-Deskhit localities, ten samples; and Tangyar, three samples) and from the Teah area, south of the Ladakh Batholith (three samples). One sample of diorite (L399) was also analysed for comparison of the lavas with the Ladakh Batholith.

These lavas form a complete differentiated suite, from basalt to rhyolite, with relatively homogeneous geochemical features, particularly concerning trace and REE patterns. Geochemical compositions of the lavas are consistent with an arc-tholeiitic to calco-alkaline evolutionary trend (Tables 2 and 4; Figs. 6 and 8). Most major element variation diagrams (Fig. 8) show an evolution from basalts with low K_2O, moderate MgO, CaO and TiO_2 and high Al_2O_3 evolving to rhyolites with high K_2O and low MgO, CaO and TiO_2. However, there is some scattering in TiO_2 and K_2O variation diagrams.

These lavas have obvious arc affinities, with LILE and Th enrichments [higher $(Th/Yb)_N$ values than Western Ladakh lavas, Fig. 6F and Table 4]. They have marked negative Nb anomalies and high LREE enrichments (see $(La/Nb)_N$, $(La/Sm)_N$ and $(La/Yb)_N$ ratios in Table 4).

Eastern Ladakh lavas have lower εNd_{110} and higher Pb isotopic ratios than Western Ladakh lavas (Fig. 7; Table 4). Isotopic data of Teah and Deskhit lavas are in the same value ranges ($0 < \varepsilon Nd < 5.5$) and εNd_{110} does not decrease as SiO_2 increases. These isotopic compositions show that the source of Eastern Ladakh lavas is notably more radiogenic than that of Western Ladakh arc lavas (Fig. 7A).

The very low εNd value of the diorite L399 ($\varepsilon Nd_{110} = -7.5$) suggests that a higher amount of crustal material was involved in the production of the later Ladakh Batholith granitoids (U–Pb ages of 63–50 Ma; Weinberg and Dunlap, 2000) and that the lavas cannot be directly related to the Ladakh Batholith, as proposed by Ahmad et al. (1998).

In summary, few remarks can be done on the basis of these results.

Western Ladakh is characterised by three different suites, all with oceanic affinities (Fig. 7B and Table 4): (1) The tholeiitic Northern Group with low La/Yb and high εNd, assumed to be emplaced in a back-arc basin;, (2) the arc-tholeiites of the Southern Group are characterised by high La/Yb, and relatively high εNd and represent the remnants of the intra-oceanic arc; and (3) the Nb–Ti rich Katzarah lavas bear high La/Yb, like the arc tholeiites, but

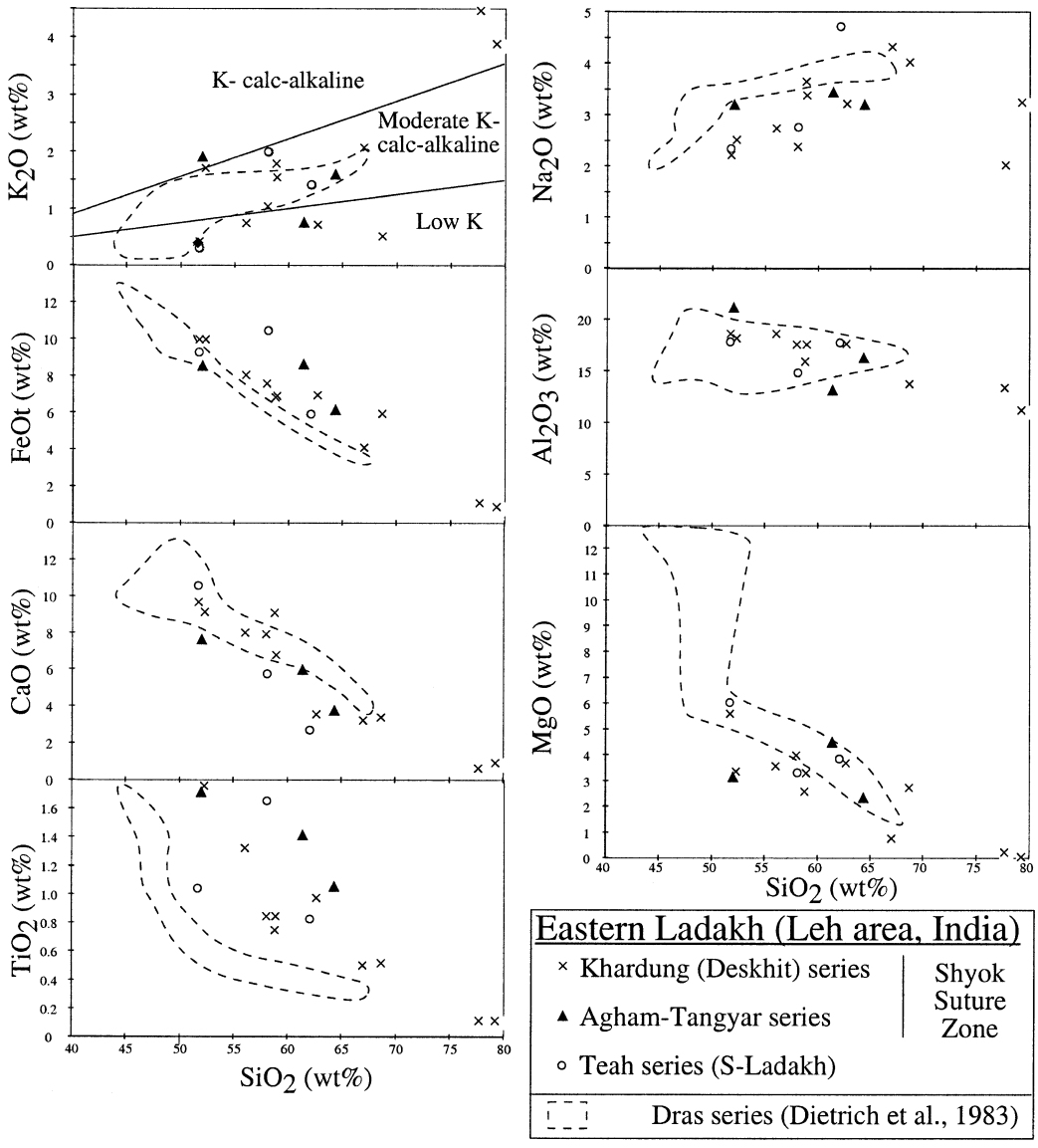

Fig. 8. Harker variation diagrams of Eastern Ladakh lavas. The field of Dras lavas (Dietrich et al., 1983) is shown for comparison.

differ by relatively lower εNd and the absence of negative Nb and Ti anomalies, similar to OIB-type lavas.

Eastern Ladakh contains a more homogeneous and differentiated volcanic arc-suite of continental affinity with lower εNd and higher La/Yb.Comparison with other Ladakh and Kohistan cretaceous volcanic suites.

On a broader scale, the geochemical features of the Ladakh volcanic suites developed here are in agreement with those of different areas from Ladakh and Kohistan, available in the literature.

- *In Ladakh*, the Dras lavas (Reibel and Juteau, 1981; Honegger et al., 1982; Dietrich et al., 1983) are mainly basalts, with no andesitic end-members, characterised by high Mg contents (MgO ~ 12 wt.%;

Table 5
Representative chemical analyses of Kohistan–Ladakh lavas and other lava types

Sample no.	SP45	CH413	CH417	HT 344	Hunza HMg	PL28	IK 1012	A83	A121	786B	KB	IR-1			Experimental adakitic liquid	P90-35
Type	Diorite	H Ti B	L Ti AB	HMB	HMB	HMAB	arc-AB	H Ti B	L Ti B	HCB	HMB	HMAB	Adakites	TTG		NRB
Ophiolite	Spong-tang	Nidar	Nidar	Dras	Chalt	Chalt	Chilas	Kamila	Kamila	Izu-Bonin	Rhyukyu	Rhyukyu	(n = 81)	(n = 355)		
Reference	Maheo et al. (2000)			Dietrich et al. (1983)	Petterson et al. (1999)	Khan et al., 1997				Pearce et al. (1992)	Shinjo (1999)		Martin (1999)		Rapp et al. (1991)	Sajona et al. (1996)
Major elements (wt.%) recalculated at 100% on an anhydrous base																
SiO_2	53.49	51.01	53.53	52.02	50.77	53.91	52.93	51.84	50.67	52.65	51.24	54.40	65.28	69.98	69.28	51.25
TiO_2	0.66	2.44	0.54	0.65	0.33	0.21	1.25	2.27	0.47	0.39	0.85	1.43	0.51	0.34	0.54	1.68
Al_2O_3	15.20	14.14	14.85	13.83	10.46	12.34	18.43	14.49	16.48	15.09	14.22	14.97	16.93	15.60	16.78	15.57
Fe_2O_3	1.64	2.18	1.28	0.06	1.52	1.45	1.43	2.23	1.35	1.34	1.50	1.67	0.64	0.47	0.44	1.78
FeO	8.34	11.14	6.54	8.78	7.73	7.42	7.29	11.36	6.88	6.86	7.63	8.49	3.24	2.39	2.25	9.05
MnO	0.17	0.24	0.13	0.17	0.18	0.19	0.12	–	–	0.12	0.15	0.18	0.08	0.05	0.09	0.39
MgO	5.15	5.38	9.05	12.33	15.11	11.46	5.35	5.17	8.24	8.04	11.14	7.55	2.22	1.18	1.25	6.92
CaO	9.59	9.24	10.67	9.21	12.03	10.42	9.52	9.75	12.37	11.41	10.33	8.67	5.05	3.20	3.90	9.52
Na_2O	5.31	3.64	3.19	1.93	1.39	2.40	2.76	2.43	2.83	2.68	2.12	2.32	4.13	4.89	4.17	3.07
K_2O	0.36	0.45	0.15	0.88	0.44	0.16	0.67	0.26	0.57	1.31	0.71	0.18	1.74	1.76	1.30	0.50
P_2O_5	0.08	0.12	0.06	0.15	0.05	0.03	0.25	0.19	0.12	0.10	0.11	0.13	0.17	0.13	0.00	0.27
(ppm)																
Ba	182	32	14	74	53	17	211	–	–	17	124	78	–	–		110
Rb	6.3	2.6	1.3	13	8.8	3.3	7.0	2.0	10.0	5.8	13.2	2.9	–	–		8.0
Sr	473	193	116	167	81	71	403	150	268	147	395	197	706	454		351
Ta	0.06	0.25	0.05	–	–	–	–	–	–	0.02	0.15	0.43	–	–		–
Th	0.13	0.16	0.06	–	1	–	–	–	–	0.12	2.37	1.08	–	–		–
Zr	25	70	22	–	24	22	71	139	23	33	72	78	–	–		102
Nb	0.79	3.18	0.65	–	0.50	1.20	3.70	4.80	1.00	0.39	2.10	6.50	–	–		12.00
Y	17.1	39.6	14.1	12	9.1	9.6	18.0	53.0	13.0	10.6	19.4	20.1	10	7.5		28.0
Hf	0.99	2.18	0.78	–	–	–	–	–	–	0.89	1.97	2.13	–	–		–
V	284	265	251	235	236	–	–	–	–	237	255	132	–	–		3
Cr	34	66	375	636	1143	936	18	–	–	404	479	207	36	29		250
Ni	23	10	113	198	266	191	3	22	56	170	171	44	24	14		190
Co	34.9	39.6	39.1	46	–	–	–	–	–	40.7	47	42	–	–		58
U	0.6	1.0	0.6	–	–	–	–	–	–	0.2	0.6	0.2	–	–		–
Sc	36.8	41.9	40.8	36	–	–	–	–	–	30.3	36.6	18.8	–	–		23
La	1.89	4.16	1.38	3.5	1.2	–	–	–	–	2.22	8.10	6.81	19	9		10.00
Ce	5.65	12.73	4.16	9.5	3.8	–	–	–	–	4.13	18.50	14.25	–	–		21.00
Pr	0.92	2.13	0.69	–	–	–	–	–	–	0.78	2.52	1.88	–	–		–
Nd	4.7	11.3	3.7	7.17	2.8	2.1	13.6	15.4	5.8	3.8	11.5	9.2	–	–		15.0
Sm	1.58	3.85	1.28	2.22	–	0.77	3.56	5.3	1.74	1.07	3.02	2.97	–	–		–
Eu	0.6	1.6	0.5	0.72	–	–	–	–	–	0.4	1.0	1.2	–	–		1.4
Gd	2.26	5.16	1.74	2.48	–	–	–	–	–	1.41	3.19	3.65	–	–		–
Tb	0.40	0.97	0.32	0.4	–	–	–	–	–	0.26	0.53	0.61	–	–		–
Dy	2.7	6.5	2.2	–	–	–	–	–	–	1.7	3.2	3.5	–	–		4.2
Ho	0.61	1.42	0.50	–	–	–	–	–	–	0.37	0.69	0.69	–	–		–
Er	1.751	4.048	1.420	–	–	–	–	–	–	1.1	2.000	1.810	–	–		2.400
Yb	1.73	3.70	1.40	1.47	–	–	–	–	–	1.14	1.89	1.44	0.93	0.50		1.70
Lu	0.26	0.55	0.21	0.24	–	–	–	–	–	0.17	0.29	0.21	–	–		–

H Ti: high Ti; L Ti: low Ti; HM: high Mg; B: basalt; AB: andesitic basalt; HCB: high Ca boninite; TTG: Tonalites–Trondhjemites–Granodiorites; NRB: niobium-rich basalt.

Table 5) with similar tholeiitic arc characteristics as the Southern Group. In south-eastern Ladakh Nidar area, two types of lavas are present (Maheo et al., 2000; Table 5). The first is TiO_2-rich (~2 wt.%) and MgO-poor (~5 wt.%), similar to I-MORB. The second differs by low-TiO_2 (~0.5 wt.%) and high-MgO (~9 wt.%) contents, with compositions close to high-Ca boninites, which is compatible with a fore-arc setting (Pearce et al., 1992). Finally, the Spongtang gabbros, with low MgO (~5 wt.%) and TiO_2 (~0.7 wt.%), are geochemically closer to N-MORB than to arc-type lavas (Maheo et al., 2000).

- *In Kohistan*, the heterogeneity of the Cretaceous volcanic and plutonic rocks has been shown by several authors (Table 5). The Chalt lavas with commonly picritic or boninitic compositions (Petterson and Windley, 1991) with high MgO (~11–16 wt.%) and CaO (~10–12 wt.%) contents, correlated with low TiO_2 (~0.2–0.3 wt.%) and Al_2O_3 (~10–13 wt.%) resembles high-Mg basalts and andesites (Kay, 1978; Shinjo, 1999; Table 5). The Kamila amphibolites have been separated in two groups by Khan et al. (1997): (1) a high-Ti group and (2) a low-Ti group, which are respectively similar to I-MORB and high-Ca boninites, and appear to be very close to the Ladakh Nidar area lavas. Finally, the Chilas gabbronorites (Khan et al., 1997 and references therein) have been shown to display relatively high TiO_2 (~1–1.2 wt.%) and Al_2O_3 (~18 wt.%), and low MgO (~5.4 wt.%) contents, and thus are close to the Southern Group and Eastern Ladakh lavas.

Consequently, similar lava types can be found on each side of the Nanga Parbat–Haramosh spur, which suggests that they were part of the same arc–back-arc lineament. The lavas are generally tholeiitic with high MgO contents, with trace elements abundances similar to boninites, high-Mg andesites or Island Arc Tholeiites, probably resulting from a high geothermal gradient beneath the arc. In the following section, we will investigate the reasons for such geochemical aspects.

5. Discussion: geochemical processes

The geochemical study of Western Ladakh lavas has revealed the presence of lavas with widely contrasting geochemical characteristics. These contrasts suggest the contribution of several sources and geochemical processes. In particular, the presence of adakitic and Nb-rich lavas suggests the contribution of melts from subducted oceanic crust (e.g. Sajona et al., 1996 and references therein). Other lavas such as high-Mg basalts and andesites, which have been described in Dras and Chilas suggest the interaction of slab melts with the overlying mantle (e.g. Shinjo, 1999). Does crustal melting played a role in the geochemical variety observed in Western Ladakh? To answer to this question, we will investigate the respective contributions of the nature of sources, partial melting and fractional crystallisation in the geochemical variety occurring in Western Ladakh.

5.1. Degree of partial melting and fractional crystallisation

In the studied area, Western Ladakh lavas show contrasted geochemical types with restricted differentiation (mainly andesitic basalts) while Eastern Ladakh lavas form a more complete differentiation series from basalts to rhyolites. Western Ladakh lavas show restricted variations in La contents at given values of La/Yb, but relatively important variations of La/Yb [$(La/Yb)_N = 0.6–56$] (Fig. 9A). These variations seem to be more related to different melting rates or sources than fractional crystallisation. Three geochemical types are distinguished within Western Ladakh lavas: arc lavas, Nb-rich lavas and adakitic lava, each with different geochemical characteristics, including different isotopic ratios (see Section 4.2.2). It is then unlikely that the lavas types could be derived each other simply by crystal fractionation.

Eastern Ladakh lavas show more horizontal $(La)_N$ variations at similar $(La/Yb)_N$ ratios (Fig. 9A). However, $(La)_N$ enrichment is not simply related to SiO_2 increase (note that some basalts, andesites, dacite and rhyolites all have high $(La)_N$). This is also illustrated in Fig. 9B, where Eastern Ladakh and Western Ladakh lavas are Compared to Dras lavas (Honegger et al., 1982; Dietrich et al., 1983). In Fig. 9B, Eastern Ladakh and Dras lavas display two trends. Trend 1 is featured by lavas that are progressively more depleted in TiO_2 with increasing La and SiO_2 (i.e., Dras lavas and part of Eastern Ladakh lavas), compatible with a fractional crystallisation

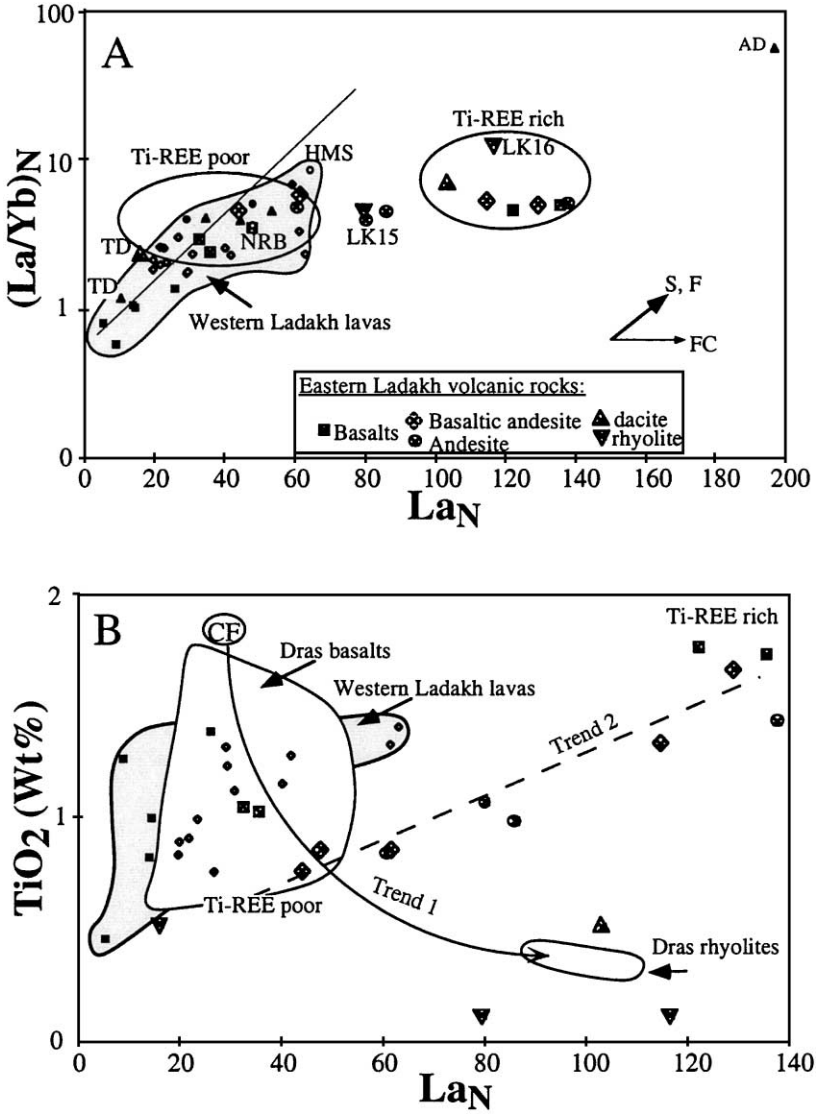

Fig. 9. (A) $(La/Yb)_N$ vs. $(La)_N$ diagram. This diagram is generally used to show the effects of Fractional crystallisation (CF) vs. the influence of the source (S) or of various partial melting rates (F). Note that silica enrichment of Eastern Ladakh lavas (featured by the series from basalts to rhyolites) is not correlated with La enrichment. (B) TiO_2 vs. $(La)_N$ diagram. This diagram compares Western and Eastern Ladakh series to the Dras series [open fields, data from Dietrich et al., 1983]. In Dras series and for some Eastern Ladakh samples, the decrease of TiO_2 from basalts to rhyolites can be explained by fractional crystallisation of Ti-phases, while La concentration increases in the residual melt. In contrast, most Eastern Ladakh samples display a good positive correlation of TiO_2 and La, unrelated to SiO_2 content, showing that fractional crystallisation cannot explain LREE enrichment. Symbols for Western Ladakh lavas are same as in Fig. 3. AD: adakitic lava, NRB: Nb-rich basalt, TD: Tholeiitic Dacite, HMS: High-Mg Shoshonitic basalt.

process of Ti-bearing phases. In contrast, Trend 2 is featured by a positive correlation of TiO_2 contents and $(La)_N$ ratios of some Eastern Ladakh lavas, these enrichments being unrelated to silica enrichment. Ti and $(La)_N$ enrichments cannot thus simply be derived by fractional crystallisation processes. However, they could be related to different melting rates and more particularly to mixing of different magma

types, as featured by important εNd variations ($0.6 < \varepsilon Nd < 5.5$; Table 3) and as also suggested by inverse zoning of plagioclase and pyroxene (see Section 4.1).

An estimate of the degree of partial melting can be obtained using a simple batch melting model, using Shaw (1970) equation:

$$C_0 = C_l(D + F(1 - D)) \quad (1)$$

D being the bulk distribution coefficient of the residual solid ($D = C_s/C_l$), C_s being the concentration of a given element in the solid residue and C_l in the liquid and F being the degree of partial melting. The modelling of partial melting processes requires determining the nature of magma sources. Considering the isotopic values, the composition of sub-arc mantle and back-arc mantle is intermediate between N-MORB and enriched mantle. Thus, the value C_0 of fertile MORB mantle (Pearce and Parkinson, 1993) has been chosen. As the degree of fractional crystallisation of a lava has been shown to be linked to the #Mg [Mg/(Mg + Fe); Klein and Langmuir, 1987], melting rate estimates will be based solely on the most primitive samples with high #Mg (> 0.6). Assuming $D_0 \approx 0$ for more incompatible elements, (1) becomes: $C_L/C_0 = 1/F$, and F values have been estimated for the most primitive lavas of each series (calculations are summarised in Table 6). Estimated partial melting values are high for all the lavas (arc-tholeiite L124: $F = 14$–16%; Back-arc lavas L156, L199: $F = 19$–21%; Katchoura lava L575: $F = 16$–21%). For all the lavas of Table 6, except the Shigar type lava, presence of residual garnet is improbable considering their flat HREE patterns. Shigar lavas display higher Sm/Yb values, consistent with the presence of garnet in the residue, consequently the F values estimates based on MREE–HREE are too high, and the value obtained with Nd and Zr (F ≈ 7–8%) should be more coherent.

5.2. Source mixing processes

The Pb, Sr and Nd isotopic ratios of Western and Eastern Ladakh lavas are in the range of the DUPAL anomaly. To represent the extent of deviation from the Northern Hemisphere Reference Line (NHRL; Hart, 1984), Pb isotopic ratios have been represented as $\Delta 7/4$ Pb and $\Delta 8/4$ Pb (Fig. 10). The DUPAL anomaly is defined by low εNd (< 7–8), high $^{87}Sr/^{86}Sr$ (> 0.704–705), high $\Delta 8/4$ ($> +60$) and high $\Delta 7/4$ ($> +8$; Hart, 1984, 1988). The isotopic compositions of the Ladakh lavas are compared to those of the Eastern Kohistan igneous rocks (Khan et al., 1997) which also display DUPAL characteristics. Khan et al. (1997) have interpreted these isotopic features as the contribution of the enriched mantle source of Indian Ocean, and proposed that Kohistan arc formed about 3000 km south of its present position. However, the DUPAL anomaly has been detected in other places along the south-eastern Asian margin (Tu et al., 1991), which suggest that this anomaly is either larger in space or more heterogeneously distributed than expected. Another alternative for these DUPAL isotopic features is that an enriched component was involved in the source of the arc at the southern Asian margin level. This enrichment could even be provided by subducted sediments as suggested for some volcanic arcs by Sun (1980) and Woodhead (1989).

Table 6
Melting rates estimates, following a simple batch melting model

Locality	–	NG	F[a]	NG	F[a]	SG	F[a]	HMS	F[a]	Shigar KF	F[a]	Katchoura KF	F[a]
Sample no.	FMM	L156		L199		L124		L144		L175		L575	
Zr	11.20	55.33	0.20	59.57	0.19	70.11	0.16	72.275	0.15	145.27	0.08	53.56	0.21
Nd	1.35	4.99	0.27	6.6	0.21	9.48	0.14	18.57	0.07	20.55	0.07	8.454	0.16
Tb	0.11	0.48	0.23	0.58	0.19	0.46	0.24	0.538	0.20	0.722	0.15	0.365	0.30
Mg#		0.60		0.61		0.67		0.67		0.69		0.80	

FMM: Fertile MORB mantle composition used in the calculation; SG: Southern Group, NG: Northern Group, KF: Katzarah Formation, Mg#: $Mg/(Mg + Fe^{2+})$.

[a] $D = 0$.

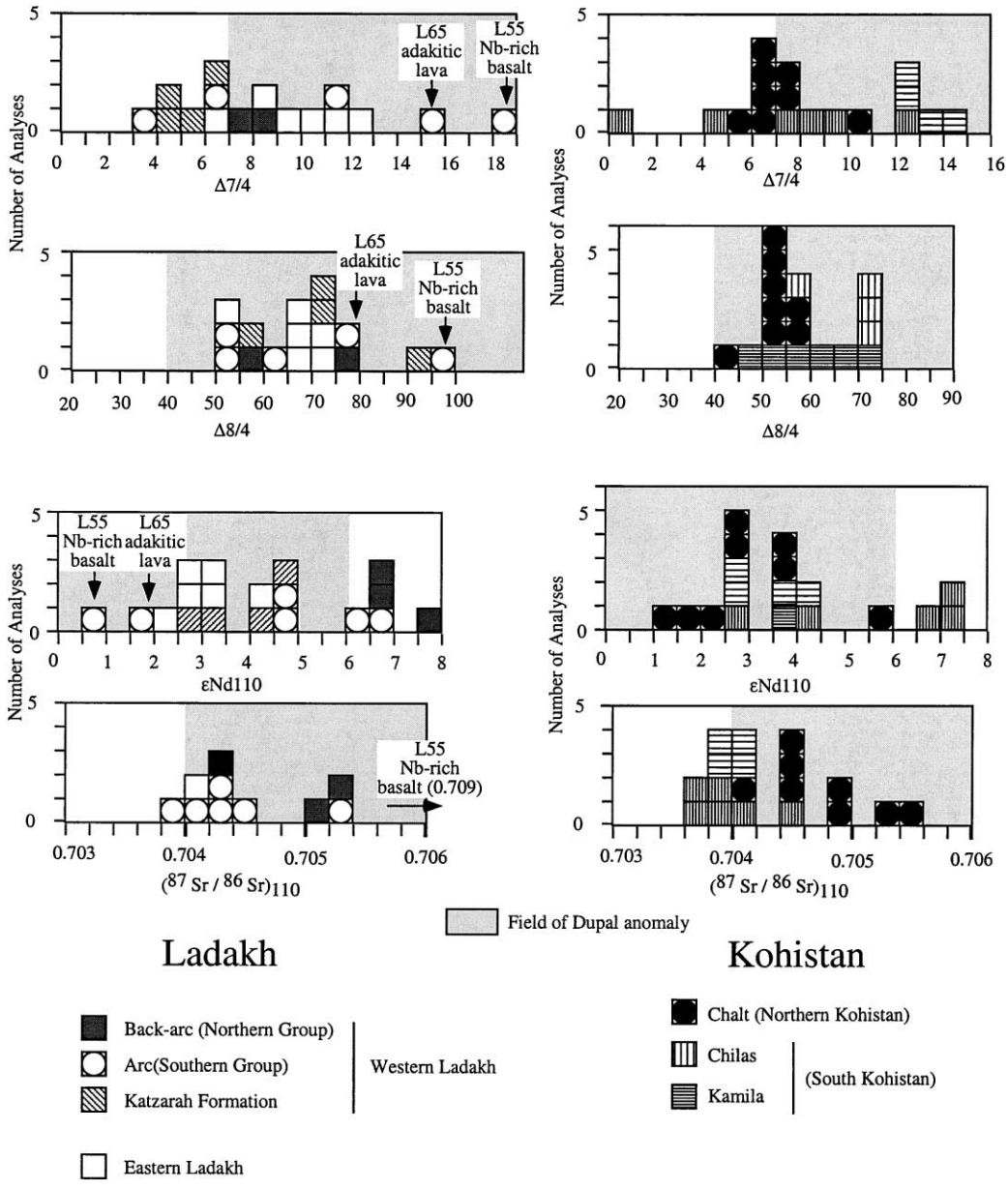

Fig. 10. Isotopic characteristics of Ladakh and Kohistan lavas. Values of Kohistan series are from Khan et al. (1997). Note that both Kohistan and Ladakh lavas have Dupal-type characteristics (shaded areas), as defined by Hart (1984).

To test which component is responsible for these radiogenic isotopic ratios, Ladakh and Kohistan (Khan et al., 1997) data are plotted with a representative set of geochemical end-members in Fig. 11. The Ladakh and Kohistan lavas plot as a sublinear field on the Fig. 11A–D (Pb vs. Pb plots), indicating that these rocks likely derived from the mixing of three components: Indian MORB Mantle, Java type pelagic sediments and Pacific Volcanogenic Sediments type components. The trends are unlikely to represent mixing trajectories with a hotspot Kerguelen-like OIB type end-member. On Fig. 11D–E, (εSr_{110} or εNd_{110} vs. $^{206}Pb/^{204}Pb$ plots) the Ladakh and Kohistan lavas define larger fields, but still the data

suggest mixing of these three components. Particularly, in the εSr_{110} vs. εNd_{110} plot (Fig. 11F), the Nb-rich basalt plots very close to the PPS end-member, showing that this lava could derive more likely from mixing of IMM with pelagic sediments than with EMII. The isotopic compositions of the Ladakh and Kohistan lavas validates the possibility of the contribution of a pelagic sediment component in the source of these rocks, as shown in particular by the Nb-rich basalt sample L55 (Fig. 11).

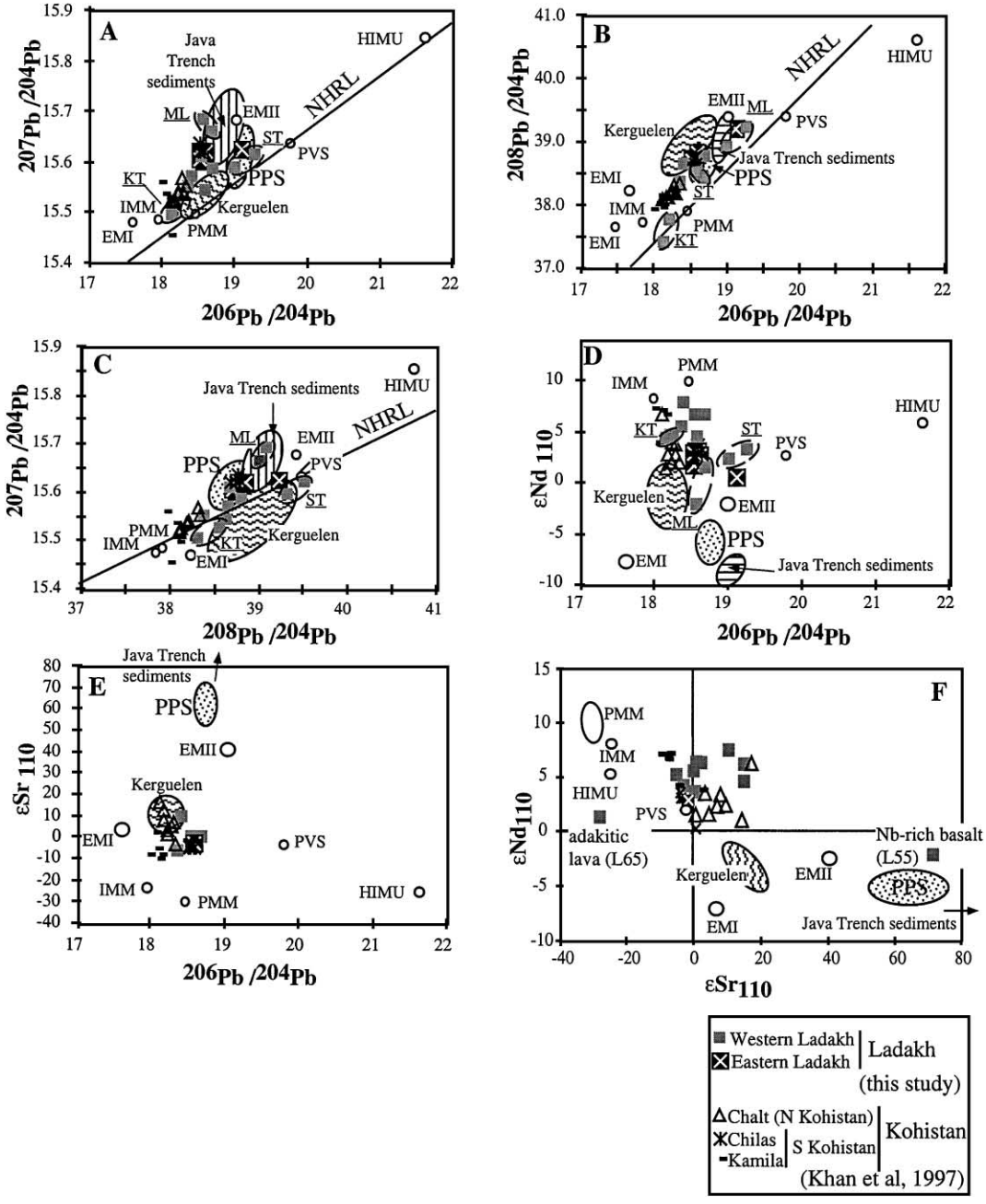

5.3. Slab and sediment melting processes, the adakite–Nb rich basalt association

Adakites are rare during island-arc volcanism, because they are formed by subducting slab melting, which require specific PT conditions (Rapp et al., 1991; Sen and Dunn, 1994). An anomalous thermal regime is necessary to reach the required pressure–temperature (P–T) conditions at which hydrated oceanic crust can melt instead of dehydrate (Peacock et al., 1994). The P–T conditions required for slab melting (Fig. 12) are several hundred degrees above "normal" conditions inferred or calculated in the subducting slab ($T > 600$°C and $P < 25$ kbar–70 km; Defant and Drummond, 1990; Drummond and Defant, 1990). Such anomalous conditions are fulfilled in the case of fast or low-angle subduction of young and hot oceanic crust (generally younger than 20 Ma).

Adakites are often associated with *Niobium-rich basalts* (Defant et al., 1992; Sajona et al., 1994, 1996; Maury et al., 1996). These basalts are generated by mantle melting, and consequently their spatial and temporal association with adakites has been interpreted as the result of mantle metasomatism by slab melts (Sajona et al., 1996). In Western Ladakh, adakitic lava and Nb-rich basalts interlayer with the Southern Group arc-tholeiites in the same locality and, they are sub-contemporaneous to arc volcanism. These two types have quite similar Pb isotopic ratios, and bear low εNd values, which are unusual in an arc context. Similar isotopic values as those of L55 Nb-rich basalt ($\varepsilon\mathrm{Nd} = -2$) have been found only in the case of Banda Arc (Fig. 7A). For Banda Arc, contribution of a continental material and pelagic sediments could explain the exceptionally high $\varepsilon\mathrm{Sr}_{110}$, ^{208}Pb, ^{207}Pb and low $\varepsilon\mathrm{Nd}_{110}$ ratios of the lavas (Vroon and Bergen, 1993; Vroon et al., 1995).

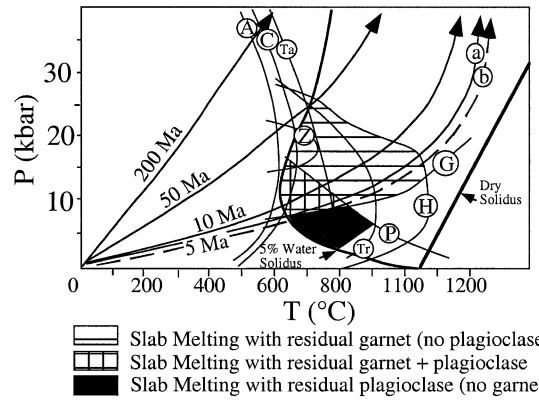

Fig. 12. Pressure (P)–temperature (T) diagram showing the calculated geotherm paths in subducted tholeiites along the Benioff plane, as a function of the age of the subducted crust (Peacock et al., 1994), after Martin (1999), modified. The main dehydration reactions are shown: A, antophyllite-out; C: chlorite-out; Ta: talc-out; Tr: tremolite-out. The lower limit of Garnet stability field is defined by G, and the upper limit of plagioclase stability field is defined by P. The 5% solidus and dry solidus curves are from Wyllie (1971) and Green (1982). Consequently, three domains of melting can be drawn, and explicated below the figure. Note that old subducted crusts (200 Ma) cross-cut the dehydration reaction curves before cross-cutting the Mantle hydrated solidus curve, whereas young crusts can cross-cut the hydrated solidus curve before complete dehydration in the garnet–plagioclase out domain (50 Ma), or in the garnet–plagioclase-in domain (10 Ma). (b) defines the effect of intense shear stresses linked to high convergence rates relative to a case of low convergence rate (a).

The experiments of Nichols et al. (1994) have shown that the hydrated solidus of clay-rich pelagic sediments is reached at 650–700°C at a 40 kbar pressure (120 km), suggesting that subducted pelagic sediments can cause melting at relatively low temperatures. These values are close to hydrated basalt solidus values obtained by Green (1982; Fig. 12), suggesting that the subducted sediments could trig-

Fig. 11. Nd, Sr, Pb isotope covariation diagrams. The mantellic end-members reported in the diagram are: Indian and Pacific MORB mantles (IMM and PMM, respectively), high U/Pb enriched mantle (HIMU) and the two Enriched Mantle components (EMI and EMII; Zindler and Hart, 1986; White et al., 1987). The range of pelagic sediment composition is defined by the following end-members: Pacific Volcanogenic Sediments (PVS), Pacific Pelagic Sediment (PPS; Ben Othman et al., 1989; Woodhead, 1989) and Java Trench sediments (Ben Othman et al., 1989). The data of the Kerguelen hotspot, representative of Indian ocean OIB source has also been plotted for comparison (Dosso and Murphy, 1980). NHRL: Northern Hemisphere Reference Line. Kohistan data is from Khan et al. (1997). Note that Ladakh and more secondarily Kohistan samples show more radiogenic ^{207}Pb/^{204}Pb and ^{208}Pb/^{204}Pb than the NHRL reference, and plot between IMM, PVS, and EMII and/or PPS end-members. Note also that particular western Ladakh lava types plot closer to these end-members. KT: Katchoura type Nb-rich lavas (L573 and L575) plot closer to IMM, ST: Shigar type Nb-rich lavas (L175 and L179) plot closer to PVS, and ML: Muchilu lavas (L55 and L65) plot closer to Java Trench sediments.

ger slab melting, which could explain the association of Nb-rich basalt–adakitic lava. However, the major, trace and isotopic compositions of the Nb-rich basalt, in particular its low Mg# (0.52) at 47 wt.% of SiO_2 are not compatible with melting of a pure mantellic source, except if melting is followed by FC of Mg-rich minerals at depth (e.i., olivine). Its anomalous composition may be due to the contribution of a Mg-poor and Ca-rich component, close to the composition of pelagic sediments. However, sediments predominantly reveal significant Nb and Ta depletions (Plank and Langmuir, 1998), thus simple sediment melting cannot account for the production of Nb-rich lavas (Johnson and Plank, 1999).

An alternative hypothesis concerning the production of Nb-rich basalts would be that the Nb enrichment is not primary, but could be due to Nb enrichment of the source via adakitic magmas (Maury et al., 1996; Sajona et al., 1996). Although Adakitic magmas are not Nb-rich, and display Nb–Ta anomalies, they are Nb-richer than slab dehydration fluids. Consequently, these melts can carry greater amounts of Nb in the mantle wedge than the fluids, via the crystallisation of Nb–Ta bearing phases (Ti-amphi-

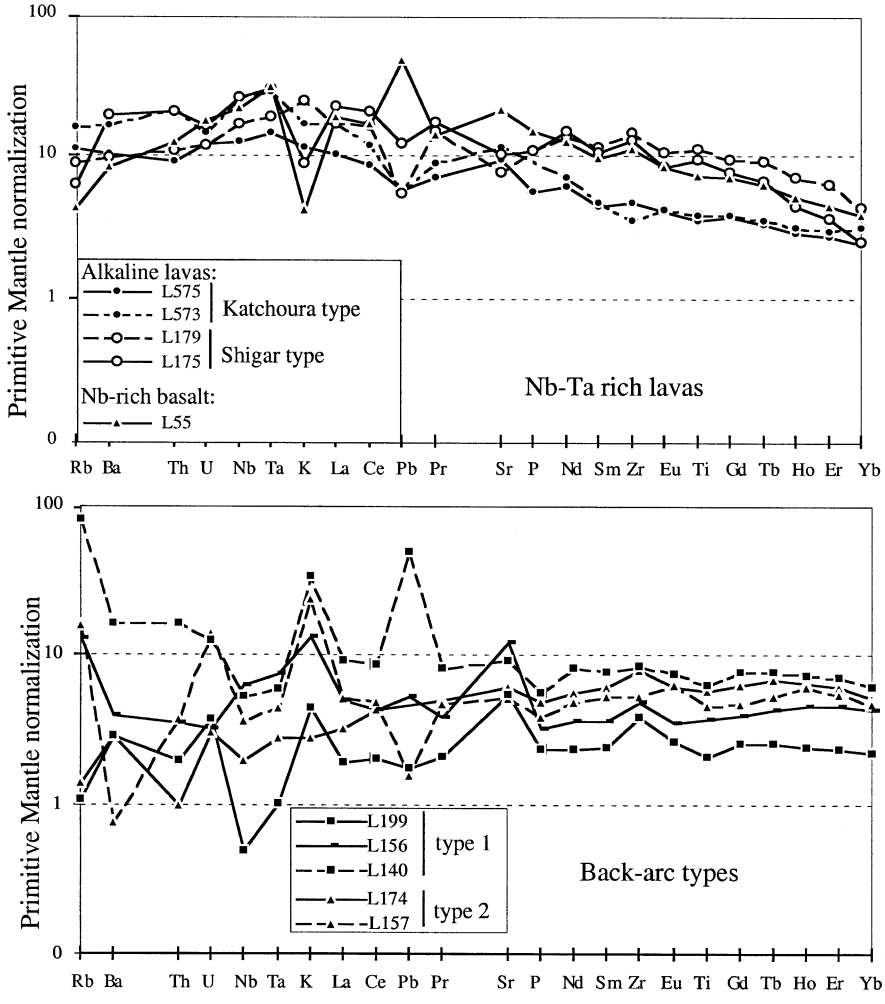

Fig. 13. Normalised Primitive Mantle diagrams of representative lavas. Normalisation values are those of Sun and MacDonough (1989). Note the similarity between Nb-rich basalt and Shigar type lavas. Note also the higher La/Yb ratio of the adakitic lava compared to Mindanao adakites (Sajona et al., 1996) shown for comparison.

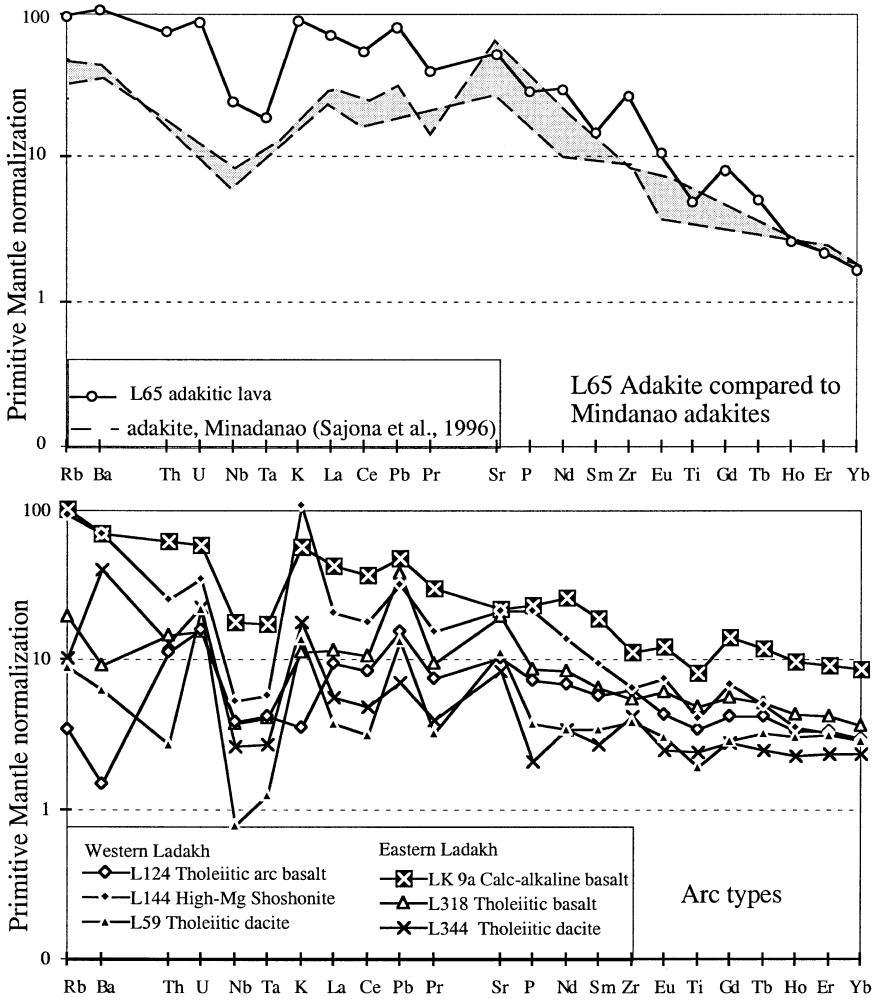

Fig. 13 (*continued*).

bole or rutile). The most acceptable hypothesis would then be that Nb-rich basalts are formed by complex interactions between ascending slab melts and the overlying mantle.

5.4. Slab melt–mantle interaction processes

Major element geochemistry of lavas produced by slab melt–mantle interaction depends strongly upon the slab melt–mantle rock volume ratio. The experiments of Rapp et al. (1999) have shown that at equal proportion of slab melt and reacting mantle, melt is fully consumed. At $\sim 2/1$ melt-reacting mantle proportions, liquids produced are Mg-rich and still silica rich. These melt–mantle interaction processes can account for the production of high-Mg basalts and andesites (Yogodzinski et al., 1995; Shinjo, 1999). Such high-Mg lavas have been documented in the Kohistan–Ladakh arc system (see Section 4). Another way to produce high-Mg lavas is the partial melting of a hydrous mantle (Kushiro, 1974; Hirose, 1997). The difference of the two processes is that the derivative liquids produced by melt–mantle interaction will keep more or less similar trace element pattern as the crustal melt (Rapp et al., 1999) whereas they would have the signature of the metasomatised mantle in the case of partial melting of hydrous mantle. All the Nb-rich lavas show quite similar

trace element patterns (Fig. 13), which favour the hypothesis of a single process of Nb enrichment of the arc source. However, Shigar and L55 Nb-rich lavas have radiogenic isotopic compositions, similar to pelagic sediments and volcanogenic sediments, while Katchoura Nb-rich lavas are much less radiogenic, and plot close to the depleted mantle end-member (IMM) (Figs. 7A,B and 11). The contribution of subducted sediments may then be more significant for Shigar and L55 basalt than for Katchoura lavas. In the case of Katchoura lavas, increased contribution of a depleted mantellic source may be due to higher percentage melting (as confirmed by the high partial melting values evaluated in Section 5.1), possibly triggered by slab melt–mantle interactions.

A quantitative evaluation of the contribution of sediments can be made, using a mixing model between an indian MORB component and pelagic sediments end-members, in a εNd vs. $^{206}Pb/^{204}Pb$ diagram (Fig. 14). As already noted by Vroon and Bergen (1993) and Vroon et al. (1995) from the case of Banda Arc, a small contribution of sediments (0.1–1%) will drastically increase $^{206}Pb/^{204}Pb$ ratios. In Fig. 14, the mixing model, even using the lowest $^{206}Pb/^{204}Pb$ ratio of Indian MORB values (17.3, Saunders et al., 1988) explains the high Pb isotopic ratios of most Ladakh lavas by 0.1–3 % mixing with pelagic sediments. Nb-rich lavas such as L55 require nearly 5% sediment contribution, while Shigar lavas would need the contribution of more radiogenic $^{206}Pb/^{204}Pb$ sediments source such as PVS or Mn-rich sediments (Ben Othman et al., 1989).

5.5. The Chang La ultramafics: behaviour of the sub-arc mantle

The composition of the Chang La orthopyroxene–spinel–olivine assemblage corresponds to an extreme case of depletion in a subduction context (Fig. 15A,B). In Fig. 15A, compositions of Chang

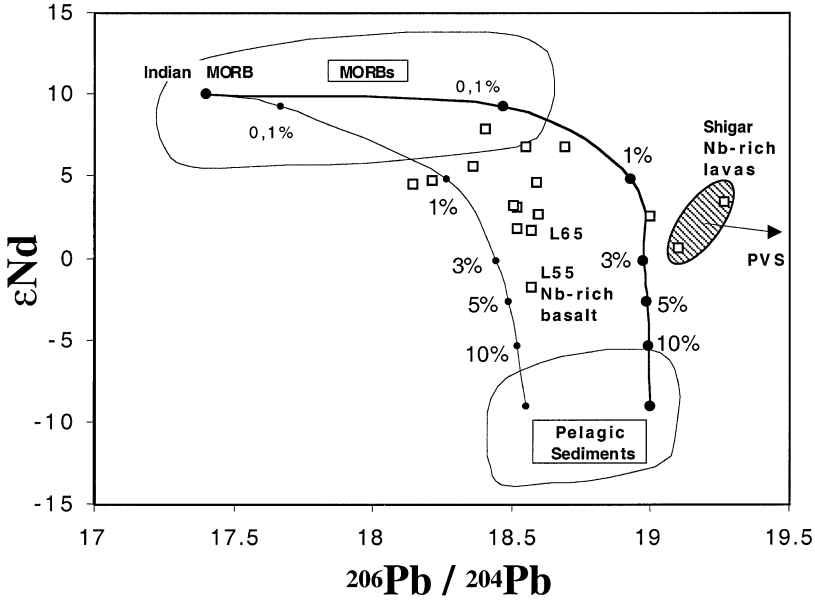

Fig. 14. εNd vs. $^{206}Pb/^{204}Pb$ mixing diagram, illustrating the proportions of sediments required to generate the isotopic compositions of Ladakh lavas. The least radiogenic compositions of the Indian MORB component ($^{206}Pb/^{204}Pb = 17.31$, $\varepsilon Nd = 10$, Pb = 0.03 ppm, Nd = 0.8 ppm; Saunders et al., 1988) and two extreme $^{206}Pb/^{204}Pb$ values of pelagic sediments ($^{206}Pb/^{204}Pb = 18.56$ and 19.00, $\varepsilon Nd = -9$, Pb = 9 and 60 ppm, Nd = 30 ppm; Ben Othman et al., 1989) are used to show the effect of pelagic sediment input to the mantle. The field of MORBs is from Saunders et al. (1988), and the field of pelagic sediments from Ben Othman et al. (1989). Note that the radiogenic Pb isotopic ratios obtained for Ladakh lavas can be obtained with a small contribution of sediments (0.1–5%), even when mixing with a depleted indian MORB end-member.

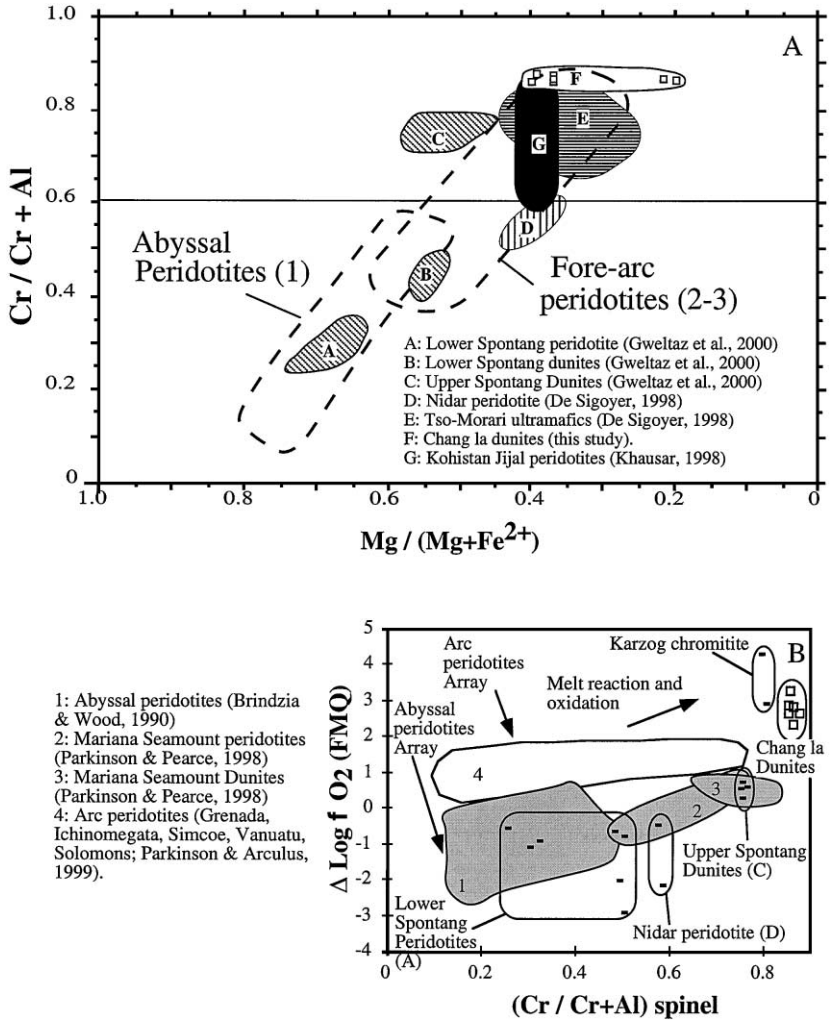

Fig. 15. Chemistry of Cr-spinel from the known ultramafic settings of Kohistan and Ladakh. (A) Cr# vs. Mg# of Cr-spinels; (B) Oxygen fugacities values (Δ logfO_2) vs. Cr# in spinel. Oxygen fugacity values were obtained with the olivine–orthopyroxene–spinel calibrations of Nell and Wood (1991), are presented relatively to the Fayalite–Magnetite–Quartz (FMQ) buffer. Values obtained for Ladakh spinels are compared with those obtained for abyssal and arc peridotites.

La spinels are compared to those of the Cretaceous southern Ladakh ultramafic rocks, exposed in the Indus Suture Zone (Tso Morari, Nidar; de Sigoyer, 1998) or obducted onto the Indian Margin (Karzog, Spongtang; Maheo et al., 2000) and to those of the southern Kohistan Jijal Complex ultramafics (Kausar, 1998). Olivine is always Fo-rich (Fo 90–97 in Spongtang, Fo $\sim$92 in Nidar and Fo $\sim$99 in Karzog) and orthopyroxene is a low-Al enstatite (En 90, $Al_2O_3 < 2$ wt.%; Maheo et al., 2000). These complexes, firstly interpreted as pure ophiolite series on the basis of their mineralogy (Reuber, 1986; Reuber et al., 1987), present some clear whole rock depletions in Ti, Cr, Ni, Ta and Nb (Maheo et al., 2000), also observed in the Chang La dunites. Such depletions are typical of supra-subductive peridotites, which are characterised by Mg-poor Cr-rich spinel, Mg-rich olivine and Mg Al-rich orthopyroxene reflecting increasing degree of partial melting (Dick and Bullen, 1984). Chang La Cr-spinels display higher Cr# and lower Mg# than those of other Kohistan and Ladakh ultramafic settings (Fig. 15A).

Olivine and orthopyroxene plot at the depleted end of the subduction margin compositional fields in the Parkinson and Pearce (1998) diagrams representing Mg# in olivine and Al_2O_3 in Orthopyroxene vs. Cr# in Spinel (not shown here). Chang La olivine–orthopyroxene–spinel assemblages yield higher equilibrium temperatures and $\Delta \log fO_2$ than other Ladakh ultramafics (Fig. 15B), with values slightly higher than those obtained for subduction margin peridotites (Parkinson and Arculus, 1999). In contrast, Spongtang to Nidar peridotites plot in the fields of abyssal and fore-arc peridotites defined by Parkinson and Pearce (1998). The positive correlation of Cr# and $\Delta \log fO_2$ can be interpreted as the result of melt extraction processes during decompression melting (Dick and Bullen, 1984; Balhaus et al., 1991), or as the effect of melt–mantle interaction (Parkinson and Arculus, 1999). The petrographical aspect of Chang La orthopyroxene as elongated and irregular crystals suggests disequilibria of orthopyroxene, interpreted by Parkinson and Arculus (1999) to reflect melt–mantle interactions. Consequently, Chang La ultramafics show clear signs of depletion that could be interpreted as the result of mantle–melt interaction processes.

5.6. Evolution towards a "normal" arc regime

The presence of Mg-rich shoshonitic lava (sample L144) and tholeiitic dacite lava (sample L59) types with transitional major and trace element patterns with adakitic lava and arc tholeiites, respectively, suggest that there could have been a spatial transition from a zone of crustal melt–mantle interaction towards a zone of " normal " arc regime. In western Ladakh, the "normal" arc regime featured by the Southern Group tholeiitic arc lavas is a primitive arc complex, characterised by lack of differentiated lavas and only slight arc features (low La/Nb and Th/La ratios). In Section 4.2.2, Eastern Ladakh lavas were shown to have relatively homogeneous geochemical features of a more evolved arc. Eastern Ladakh lavas display higher Th/Yb ratios (Table 4). This Th enrichment can be correlated to lower εNd and higher $\Delta 7/4$ and $\Delta 8/4$ ratios. These enrichments and crustal affinities found in Eastern Ladakh could be linked to an increasing contribution of subducted continental-type sediments in the source, as an increasing proportion of such sediments (sandstones) are found in the field, or could be due to the presence of a crustal basement beneath the arc (Rolland et al., 2000). However, two geochemical types are found in Eastern Ladakh (a high Ti-REE enriched type and a low Ti-REE depleted type; see Section 5.1). These two types are also found in southern Ladakh (Nidar) or southern Kohistan (Kamila). They may reflect magma mixing of crustal-type melts (Ti and trace enriched) with sub-arc mantle melts (Ti and trace depleted). These different magma compositions may also be explained by slab melt–mantle interactions (the slab melts providing REE and Ti to the mantle).

6. Genetic model for the Ladakh arc

The Shyok Suture Zone of Western Ladakh is a south-vergent tectonic pile, in which the uppermost tectonic units correspond to back-arc basin formations and lowermost units to arc formations (Rolland et al., 2000). From the field and geochemical data, a reconstituted cross-section of the volcanic arc can be made, from the fore-arc (Katzarah Formation) to the back-arc (Northern Group; Fig. 16).

Nb-rich lavas predominate in the lower part of the tectonic pile (Katzarah Formation), but are also found interlayered with Southern Group tholeiitic arc lavas in the central part of the tectonic pile (Muchilu area). This spatial distribution is indicative of a spatial transition from Nb-rich volcanism in the front of the arc to Nb-depleted volcanism in the arc itself.

The Katchoura lavas are produced by intense partial melting of mantle ($F \sim 15$–20%), in probable consequence of mantle interaction with Nb-rich hydrated melts. Adakitic lavas, formed by subducted slab melting, would explain mantle wedge Nb enrichment. Stability of garnet in the source could account for HREE depletions of adakitic lava L65, while unstability of rutile (or other Nb acceptor phases) in the mantle wedge could account for the absence of Nb–Ta anomalies in Nb-rich lavas (e.g. Sajona et al., 1996; Kelemen et al., 1993). The presence of heterogeneous lava types, Mg-poor Nb-rich and adakitic lavas interlayers within tholeiitic arc Southern Group, suggests less efficient melt–mantle mixing and a spatial transition towards a

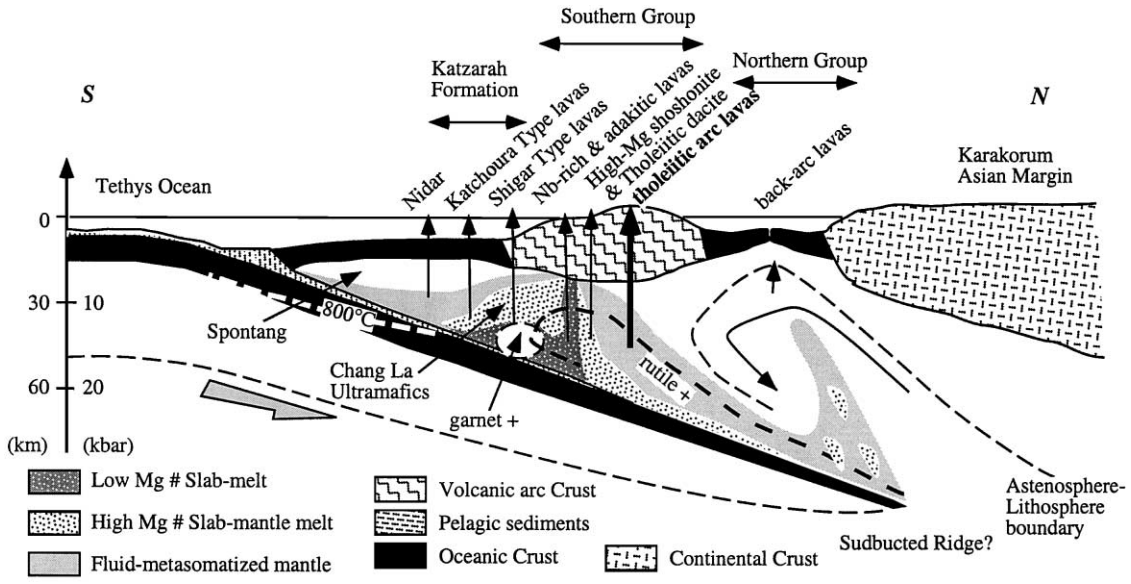

Fig. 16. Proposed genetic model of the Western Ladakh volcanic arc in Mid-Cretaceous Albian–Aptian times.

"normal" arc regime. Nevertheless the "normal" arc regime is featured by still high rate melting ($F \sim 15\%$) of a slightly depleted mantle source. Northern Group back-arc basin lavas are compatible with higher rate melting ($F \sim 20\%$) of a more depleted mantellic source. Nevertheless, these lavas still show important geochemical variations that could be explained by source heterogeneity under the back-arc basin region. These heterogeneities could be due to efficient mantle convecting under the back-arc basin, probably linked to the rapid India–Asia convergence.

In Eastern Ladakh, the relative geochemical homogeneity of the lavas could be due to more important mixing of the different end-members individualised in Western Ladakh, and to a thicker arc complex.

7. Geodynamic implications for the Middle Cretaceous tectonic context of the Kohistan–Ladakh arc series

From the data presented here, we interpret the Kohistan and Ladakh Albian–Aptian series as a coherent and complete volcanic arc series. Most Middle Cretaceous Kohistan–Ladakh lavas display high MgO contents, with frequently picritic compositions. Their composition is close to high-Mg basalts and basaltic andesites and/or boninites (Table 5). The geochemical diversity of this arc can be explained by relatively high melting rates, probably due to a high geothermal gradient, and by mixing processes between at least two components (IMM-Pelagic sediments and PVS), and more secondarily by variable levels of fractional crystallisation. We consequently propose that the DUPAL-type isotopic ratios represent enrichment linked to the assimilation of pelagic sediments (Fig. 14), close to Nb-rich basalts composition rather than to a primary mantle composition. As the DUPAL-type anomaly can be explained by such mixing processes, we suggest that it cannot be used for a geodynamic reconstitution such that proposed by Khan et al. (1997). However, the spread of the DUPAL-type isotopic anomaly, between the Asian and Indian plates in Mid-Cretaceous times, is not well constrained for such a reconstitution.

In Middle Cretaceous times, the Kohistan–Ladakh arc may have belonged to a complex and unique arc series, formed along the Asian margin in response to the northward subduction of the Neo-Tethys Ocean. The isotopic composition of the lavas, the presence of adakitic and Nb-rich lava types and the petrology of mantle relicts suggest interactions of crustal melts

with a slightly depleted mantle (IMM-EMII). High melting rates and crustal melting imply a high geothermal gradient ($T > 700$°C at $P < 17$ kbar, Fig. 12). The thermo-barometric conditions required in the case of slab melting are those prevailing in a young (< 15–20 Ma) subducted crust. Nb–Ti-rich and adakitic lavas are currently described in arc tectonic settings where a young (< 5 Ma) oceanic crust is being subducted (Solomon Islands: Petterson et al., 1999; Mindanao island: Sajona et al., 1996; Maury et al., 1996; Cascade Range: Leeman et al., 1990; Taitao Peninsula: Bourgois et al., 1996; Guivel et al., 1999). Two major tectonic events may be combined to explain the subduction of such a young lithosphere. Prior to the arc formation (1) the rapid subduction of the Paleo/Meso Tethys Ocean, north of the Tibetan Lhasa block, has lead to the accretion of this block against the Asian margin in Lower-Middle Cretaceous (Besse et al., 1984; Fig. 17A). This accretion has blocked the only free (Asian) boundary of the Tethyan system, whereas (2) intense north-vergent stresses prevailed on its southern (Indian) boundary, due to the initiation of the fast northward drift of the Indian Plate also in Lower–Middle Cretaceous times. In this context of rapid plate motion inversion, the oceanic ridge would have been the weakest plate boundary, where subduction could be more easily initiated (Fig. 17B). These data are therefore compatible with the eastward prolongation of the subduction close to the ridge invoked for the initiation of the Oman obduction (Coleman, 1981; Boudier and Coleman, 1981). Following this model, the Kohistan–Ladakh arc system was built in response to northward subduction of Neo-Tethys ocean (Fig. 17C). The lateral asymmetry found between western Ladakh (arc + back-arc in a marine environment) and eastern Ladakh (evolved arc in a sub-continental environment) suggests subduction oblique to the Asian margin (Rolland et al., 2000). Consequently (Fig. 17C), the arc system formed intra-oc-

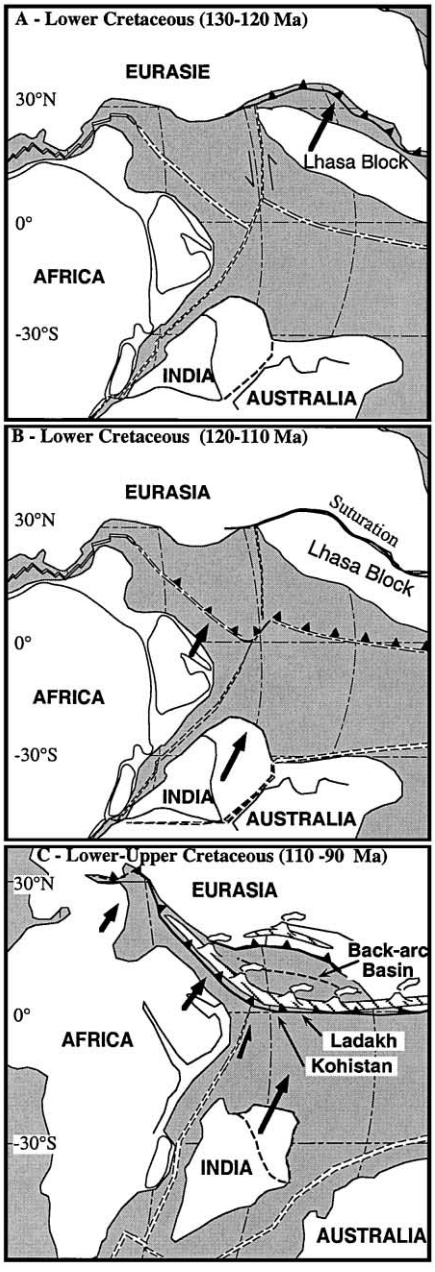

Fig. 17. Tectonic reconstitution proposed for (A–B) the Lower–Middle Cretaceous initiation of the India–Asia convergence, and (C) Kohistan–Ladakh arc formation. The approximate relative positions of continents are from Scotese and Golonka (1992) and Van der Voo et al. (1999). The position of the Lhasa block is from Sengör and Natal'in (1996). The form of the Indian continent is from Matte et al. (1997). The position of Neo-Tethys ridge is inferred from the relative positions of Lhasa and India, and from the emplacement and timing of Oman ophiolite obduction (Coleman, 1981; Boudier and Coleman, 1981). Double strippled lines represent mid-oceanic ridges, single bold lines with plain triangles represent subduction zones, hatched domains correspond to volcanic arc lineaments and arrows represent direction and norm of tectonic blocks motions (Patriat and Achache, 1984).

eanically in the west (close to the Oman ophiolite) could have prolonged to an Andean type margin in the east (active Tibetan continental margin).

Consequently, we propose that the wide-scale inversion of the tectonic divergent opening of the Neo-Tethys Ocean, due to the fast northward drift of the Indian Plate initiated in Early–Middle Cretaceous, has induced the subduction of the Neo-Tethys mid-oceanic ridge. This hypothesis is also supported by large-scale ophiolite obductions which have occurred on both the Arabic (Oman) and Indian (Kohistan–Ladakh) margins, probably due to the coupling of the continental plates with their respective subducting oceanic plates.

Acknowledgements

This work has been financially supported by LGCA-UMR 5025, and was conducted in collaboration with the Geosciences Laboratory of Islamabad (Pakistan), with the help of the French Embassy in Pakistan. We particularly thank Mr. Hasan Gohar, Mr. M. Sakhawat, Mr. Tahir Karim and Mr. A.B. Kausar from Geosciences Laboratory and the French councillor, Mr. Desseix, from the French Embassy for their involvement. Special thanks are due to N. Arndt for his critical review of the manuscript and journal reviewers S.L. Chung, H. Martin and M. Petterson. We also thank T. Khan and C. Chauvel for discussions, and P. Brunet and P. Telouk for their assistance in obtaining the isotopic Pb, Sr and Nd data.

References

Ahmad, T., Thakur, V.C., Islam, R., Khanna, P.P., Mukherjee, P.K., 1998. Geochemistry and geodynamic implications of magmatic rocks from the Trans-Himalayan arc. Geochem. J. 32, 383–404.

Balhaus, C., Berry, R.F., Green, D.H., 1991. High pressure experimental calibration of the olivine–orthopyroxene–spinel oxygen barometer: implications for the oxidation state of the mantle. Contrib. Mineral. Petrol. 107, 27–40.

Bard, J.P., Maluski, H., Matte, P., Proust, F., 1980. The Kohistan sequence: crust and mantle of an obducted island arc. Geol. Bull. Univ. Peshawar Spec. Issue 13, 87–94.

Barrat, J.A., Keller, F., Amossé, J., Taylor, R.N., Nesbitt, R.W., Hirata, J., 1996. Determination of rare earth elements in sixteen silicate samples by ICP-MS after Tm addition and Im exchange separation. Geostand. Newsl. 20, 133–139.

Ben Othman, D., White, W.M., Patchett, J., 1989. The geochemistry of marine sediments, island arc magma genesis and crust–mantle recycling. Earth Planet. Sci. Lett. 94, 1–21.

Besse, J., Courtillot, V., Pozzi, J.P., Westphal, M., Zhou, Y.X., 1984. Paleomagnetic estimates of crustal shortening in the Himalayan thrusts and Zangbo suture. Nature 311, 621–626.

Boudier, F., Coleman, R.G., 1981. Cross-section through the peridotites in the Semail ophiolite, Southeastern Oman. J. Geophys. Res. 86, 2573–2592.

Bourgois, J., Martin, H., Lagabrielle, Y., Le Moigne, J., Frutos Jara, J., 1996. Subduction erosion related to spreading ridge subduction: taito peninsula (Chile margin triple junction area). Geology 24, 723–726.

Coleman, R.G., 1981. Tectonic setting for ophiolite obduction in Oman. J. Geophys. Res. 86, 2497–2508.

Coulon, C., Maluski, H., Bollinger, C., Wang, S., 1986. Mesozoic and Cenozoic volcanic rocks from central and southern Tibet: ^{39}Ar–^{40}Ar dating, petrological characteristics and geodynamical significance. Earth Planet. Sci. Lett. 79, 281–302.

Defant, M.J., Drummond, M.S., 1990. Derivation of some modern arc magmas by melting of young subducted lithosphere. Nature 347, 662–665.

Defant, M.J., Jackson, T.E., Drummond, M.S., de Boer, J.Z., Bellon, H., Feigenson, M.D., Maury, R.C., Stewart, R.H., 1992. The geochemistry of young volcanism throughout western Panama and southeastern Costa Rica: an overview. J. Geol. Soc. (London) 149, 569–579.

De Terra, 1935. Geological studies in the northwest Himalaya between Kashmir and Indus valleys. Mem. Conn. Acad. Arts Sci. 8, 18–76.

Dick, H.J.B., Bullen, T., 1984. Chromian spinel as a petrogenetic indicator in abyssal and alpine-type peridotites and spatially associated lavas. Contrib. Mineral. Petrol. 86, 54–76.

Dietrich, V., Frank, W., Gansser, A., Honneger, K.H., 1983. A Jurassic–Cretaceous island arc in the Ladakh–Himalayas. J. Volcanol. Geotherm. Res. 18, 405–433.

Desio, A., 1974. Karakorum mountains. In: Spencer, A.M. (Ed.), Mesozoic–Cenozoic Orogenic Belts, Data For Orogenic Studies. Geol. Soc. London Spec. Publ., vol. 4, pp. 255–266.

De Sigoyer, J., 1998. Mécanismes d'exhumation des roches de haute pression basse température en contexte de convergence continentale (Tso Morari, NO Himalaya). PhD thesis, Univ. Claude Brenard-Lyon 1, France.

Dosso, L., Murphy, V.R., 1980. A Nd isotopic study of the Kerguelen islands: inferences on enriched mantle sources. Earth Planet. Sci. Lett. 48, 268–276.

Drummond, M.S., Defant, M.J., 1990. A model for trondhjemite–tonalite–dacite genesis and crustal growth via slab melting: Archean to modern comparisons. J. Geophys. Res. 95, 21503–21521.

Evensen, N.M., Hamilton, P.J., O'Nions, R.K., 1978. Rare earth abundances in chondritic meteorites. Geochim. Cosmochim. Acta 42, 1199–1212.

Green, T.H., 1982. Anatexis of mafic crust and high pressure crystallisation of andesite. In: Thrope, R.S. (Ed.), Andesites. Wiley, New York, pp. 465–486.

Guivel, C., Lagabrielle, Y., Bourgois, J., Maury, R.C., Fourcade, S., Martin, H., Arnaud, N., 1999. New geochemical constraints for the origin of ridge-subduction-related plutonic and volcanic suites from the Chile Triple Junction (Taitao Peninsula and site 862, LEG ODP141 on the Taitao Ridge). Tectonophysics 311, 83–111.

Hart, S.R., 1984. A large-scale isotopic anomaly in the Southern hemisphere mantle. Nature 309, 753–757.

Hart, S.R., 1988. Heterogeneous mantle domains: signatures, genesis and mixing chronologies. Earth Planet. Sci. Lett. 90, 273–296.

Hawkesworth, C.J., Gallagher, K., Hergt, J.M., McDermott, F., 1994. Destructive plate margin magmatism: geochemistry and melt generation. Lithos 33, 169–188.

Hirose, K., 1997. Melting experiments on lherzolite KLB-1 under hydrous conditions and generation of high-magnesian andesitic melts. Geology 25, 42–44.

Honegger, K.H., Dietrich, V., Frank, W., Gansser, A., Thommsdorf, M., Thommsdorf, K., 1982. Magmatism and metamorphism in the Ladakh Himalayas. Earth Planet. Sci. Lett. 60, 253–292.

Honegger, K.H., 1983. Strukturen und Metamorphose in the Zanskarkristallin, PhD thesis, E.T.H. Zürich, Switzerland.

Jaques, A.L., Green, D.H., 1980. Anhydrous melting of peridotite at 0–15 kb pressure and the genesis of tholeiitic basalts. Contrib. Mineral. Petrol. 73, 287–310.

Johnson, M.C., Plank, T., 1999. Dehydration and Melting Experiments Constrain the Fate of Subducted Sediments. G-cubed, http://146.201.254.53/http://146.201.254.53/.

Kausar, A.B., 1998. L'Arc Sud Kohistan, N Pakistan: Evolution Petrologique et distribution des éléments et minéraux du groupe du platine, PhD thesis, Univ. Grenoble, France.

Kay, R.W., 1978. Aleutians magnesian andesites: melts from subducted Pacific Ocean crust. J. Volcanol. Geotherm. Res. 4, 117–132.

Kelemen, P.B., Shimizu, N., Dunn, T., 1993. Relative depletion of niobium in some arc magmas: partitionning of K, Nb, La and Ce during melt–rock reaction in the upper mantle. Earth Planet. Sci. Lett. 120, 111–134.

Khan, T., Khan, M.A., Jan, M.Q., Naseem, M., 1996. Back-arc basin assemblages in Kohistan, Northern Pakistan. Geodin. Acta 9, 30–40.

Khan, M.A., Stern, R.J., Gribble, R.F., Windley, B.F., 1997. Geochemical and isotopic constraints on subduction polarity, magma sources, and palaeogeography of the Kohistan intra-oceanic arc, northern Pakistan Himalaya. J. Geol. Soc. (London) 154, 935–946.

Kushiro, I., 1974. Melting of hydrous upper mantle and possible generation of andesitic magma: an approach from synthetic systems. Earth Planet. Sci. Lett. 22, 294–299.

Lapierre, H., Dupuis, V., Mercier de Lépinay, B., Tardy, M., Ruiz, M., Maury, R.C., Hernandez, J., Loubet, M., 1999. Is the lower Duarte Igneous Complex (Hispaniola) a remnant of the Caribean plume-generated oceanic plateau? J. Geol. 105, 111–120.

Leeman, W.P., Smith, D.R., Hildreth, W., Palacz, Z., Rogers, N., 1990. Compositional diversity of Late Cenozoic basalts in a transect across the Washigton Cascades: implications for subduction zone magmatism. J. Geophys. Res. 95, 19561–19582.

Leterrier, J., Maury, R.C., Thonon, P., Girard, D., Marchal, M., 1982. Clinopyroxene composition as a method of identification of the magmatic affinities of paleo-volcanic series. Earth Planet. Sci. Lett. 120, 139–154.

Maheo, G., Bertrand, H., Guillot, S., Mascle, G., Pecher, A., Picard, C., De Sigoyer, J., 2000. Témoins d'un arc immature téthysien dans les ophiolites du Sud-Ladakh (NW Himalaya, Inde). C. R. Acad. Sci. Paris 330, 289–295.

Manhès, G., Allègre, C.J., Dupré, B., Hamelin, B., 1978. Lead–lead systematics, the age and chemical evolution of the Earth in a new representation space. Open File Rep. U.S. Geol. Surv.

Martin, H., 1986. Effect of steeper Archaean geothermal gradient on geochemistry of subduction-zone magmas. Geology 14, 753–756.

Martin, H., 1999. Adakitic magmas: modern analogues of Archaean granitoids. Lithos 637, 1–19.

Matte, P., Mattauer, M., Olivet, J.M., Griot, D.A., 1997. Continental subduction beneath Tibet and the Himalayan orogeny: a review. Terra Nova 9, 264–270.

Maury, R.C., Sajona, F.G., Pubellier, M., Bellon, H., Defant, M., 1996. Fusion de la croûte océanique dans les zones de subduction/collision récentes: l'exemple de Mindanao (Philippines). Bull. Soc. Geol. Fr. 167, 579–595.

Mikoshiba, M.U., Takahashi, Y., Takahashi, Y., Kausar, A.K., Khan, T., Kubo, K., Shirahase, T., 1999. Rb–Sr isotopic study of the Chilas Igneous Complex, Kohistan, northern Pakistan. In: Macfarlane, A., Sorkabi, R.B., Quade, J. (Eds.), Himalaya and Tibet: Mountain Roots to Mountain Tops: Boulder, Colorado, pp. 47–57. Geological Society of America Special Paper 328.

Nash, W.P., Crecraft, H.R., 1985. Partition coefficients for trace elements in silicic magmas. Geochim. Cosmochim. Acta 49, 2309–2322.

Nichols, G.T., Wyllie, P.J., Stern, C.R., 1994. Subduction zone melting of pelagic sediments constrained by melting experiments. Nature 371, 785–788.

Nell, J., Wood, B.J., 1991. High-temperature electrical measurements and thermodynamic properties of Fe_2O_3–$Fe_4Cr_2O_4$–$MgCr_2O_4$–$FeAl_2O_4$ spinels. Am. Mineral. 76, 405–426.

Parkinson, I.J., Pearce, J.A., 1998. Peridotites from the Izu–Bonin–Mariana forearc (ODP Leg 125): evidence for mantle melting and melt–mantle interaction in a supra-subductive zone setting. J. Petrol. 39, 1577–1618.

Parkinson, I.J., Arculus, R.J., 1999. The redox state of subduction zones: insights from arc-peridotites. Chem. Geol. 160, 409–423.

Patriat, P., Achache, J., 1984. India–Eurasia collision chronology has implications for crustal shortening and driving mechanisms of plates. Nature 311, 615–621.

Peacock, S.M., Rushmer, T., Thompson, A.B., 1994. Partial melting of subducting oceanic crust. Earth Planet. Sci. Lett. 121, 227–244.

Pearce, J.A., Parkinson, I.J., 1993. Trace element models for

mantle melting: application to volcanic arc petrogenesis. In: Prichard, H.M., Alabaster, T., Harris, N.B.W., Neary, N.B.W. (Eds.), Magmatic Processes and Plate Tectonics. J. Geol. Soc. London Spec. Publ., vol. 76, pp. 373–403.

Pearce, J.A., Thirlwall, M.F., Ingram, G., Murton, B.J., Arculus, R.J., Van der Laan, S.R., 1992. Isotopic evidence for the origin of Boninites and related rocks drilled in the Izu-Bonin (Ogasawara) forearc, Leg 125. In: Fryer, P., Pearce, J.A., Stokking, L. (Eds.), Proceedings of the Ocean Drilling Program. Scientific Results, vol. 125, pp. 237–261.

Petterson, M.G., Windley, B.F., 1985. Rb–Sr dating of the Kohistan arc-Batholith in the Trans-Himalaya of N. Pakistan and tectonic implications. Earth Planet. Sci. Lett. 74, 45–75.

Petterson, M.G., Windley, B.F., 1991. Changing source regions of magmas and crustal growth in the Trans-Himalayas: evidence from the Chalt volcanics and Kohistan Batholith, Kohistan, northern Pakistan. Earth Planet. Sci. Lett. 102, 326–341.

Petterson, M.G., Babbs, T., Neal, C.R., Mahoney, J.J., Saunders, A.D., Duncan, R.A., Tolia, D., Magu, R., Qopoto, C., Mahoa, H., Natogga, D., 1999. Geological-tectonic framework of Solomon Islands, SW Pacific: crustal accretion and growth within an intra-oceanic setting. Tectonophysics 301, 35–60.

Pudsey, C.J., 1986. The Northern Suture, Pakistan, margin of a Cretaceous island arc. Geol. Mag. 123, 405–423.

Rai, H., 1983. Geology of the Nubra Valley and its significance on the evolution of the Ladakh Himalaya. In: Thakur, V.C., Sharma, K.K. (Eds.), Geology of Indus Suture Zone of Ladakh. Wadia Institute of Himalayan Geology, Dehra Dun, pp. 79–97.

Rapp, R.P., Watson, E.B., Miller, C.F., 1991. Partial melting of amphibole/eclogite and the origin of Archean trondhjemites and tonalites. Precambrian Res. 94, 4619–4633.

Rapp, R.P., Shimizu, N., Norman, M.D., Applegate, G.S., 1999. Reaction between slab-derived melts and peridotite in the mantle wedge: experimental constrains at 3.8 Gpa. Chem. Geol. 160, 335–356.

Raz, U., Honegger, K., 1989. Magmatic and tectonic evolution of the Ladakh Block from field studies. Tectonophysics 161, 107–118.

Reuber, I., 1986. Geometry of accretion and oceanic thrusting of the Spongtang Ophiolite,Ladakh-Himalaya. Nature 321, 592–596.

Reuber, I., 1989. The Dras Arc: two successive volcanic events on eroded oceanic crust. Tectonophysics 161, 93–106.

Reuber, I., 1990. Les ophiolites de la Shyok dans l'Himalaya du Ladakh: reliques de la plaque océanique de la Neo-Neo-Tethys surmontée d'un arc volcano-sédimentaire daté du Crétacé moyen. C. R. Acad. Sci. Paris 310, 1255–1262.

Reuber, I., Colchen, M., Mevel, C., 1987. The geodynamic evolution of the South-Tethyan margin in Zanskar, NW-Himalaya, as revealed by the Spongtang ophiolitic melanges. Geodin. Acta 1, 283–296.

Rolfo, F., 1998. Evoluzione tettono-metamorfica di orogeni collisionali: l'esempio del Cristallino dell'Alto Himalaya, dell'Arco del Ladakh (Pakistan settentrionale) e del Dabie Shan (Cina centro-orientale), PhD thesis, Consorzio Universitario Torino-Genova-Cagliari, Italy.

Rolfo, F., Lombardo, B., Compagnoni, R., Le Fort, P., Lemmenicier, Y., Pêcher, A., 1997. Geology and metamorphism of the Ladakh Terrane and Shyok Suture Zone in the Chogo Lungma-Turmik area (northern Pakistan). Geodin. Acta 10, 251–270.

Rolland, Y., Pêcher, A., Picard, C., 2000. Mid-Cretaceous Back-arc formation and Arc evolution along the Asian margin: the Shyok Suture Zone in northern Ladakh (NW Himalaya). Tectonophysics.

Sajona, F.G., Bellon, H., Maury, R.C., Pubellier, M., Cotten, J., Rangin, C., 1994. Magmatic response to abrupt changes in geodynamic settings: pliocene-Quaternary calc-alkaline and Nb-enriched lavas from Mindanao (Philippines). Tectonophysics 237, 47–72.

Sajona, F.G., Maury, R.C., Bellon, H., Cotten, J., Defant, M., 1996. High field strength element enrichment of pliocene–pleistocene island arc basalts, Zamboanga Peninsula, Western Mindanao (Philippines). J. Petrol. 37, 693–725.

Schaltegger, U., Zeilinger, G., Frank, M., Burg, J.P., 2000. Formation of juvenile island arc crust through melting of sub-arc mantle: precise U–Pb Aages and Hf isotopes from a fossil crust–mantle transition in the Kohistan complex (Northern Pakistan). Journal of Conference Abstracts of Goldschmidt Conference, vol. 5 (2) Cambridge Publications, p. 885.

Schärer, U., Hamet, J., Allègre, C.J., 1984. The Transhimalaya (Gangdese) plutonism in the Ladakh region: a U–Pb and Rb–Sr study. Earth Planet. Sci. Lett. 67, 327–339.

Scotese, C.R., Golonka, J., 1992. Paleomap Paleogeographic Atlas. Paleomap Project. Univ. Texas, Arlington, 33 pp.

Sen, C., Dunn, T., 1994. Dehydration melting of a basaltic composition amphibolite at 1.5 and 2.0 Gpa: implications for the origin of adakites. Contrib. Mineral. Petrol. 119, 394–409.

Sengör, A.M.C., Natal'in, B.A., 1996. Paleotectonics of Asia: fragments of a synthesis. In: Yin, A., Harrison, M. (Eds.), The Tectonic Evolution of Asia. Cambridge Univ. Press, Cambridge, pp. 486–640.

Shaw, D.M., 1970. Trace element fractionation during anatexis. Geochim. Cosmochim. Acta 34, 237–243.

Shinjo, R., 1999. Geochemistry of high Mg andesites and the tectonic evolution of the Okinawa Trough–Ryukyu arc system. Chem. Geol. 157, 69–88.

Sullivan, M.A., Windley, B.F., Saunders, A.D., Haynes, J.R., Rex, D.C., 1994. A paleogeographic reconstruction of the Dir Group: evidence for magmatic arc migration within Kohistan, N. Pakistan. In: Treloar, P.J., Searle, M.P. (Eds.), Himalayan Tectonics. Geol. Soc. London Spec. Publ., vol. 74, pp. 139–160.

Sun, S.S., 1980. Lead isotopic study of young volcanic rocks from mid-ocean ridges, ocean islands and islands arcs. Philos. Trans. R. Soc. London 297, 409–455.

Sun, S.S., McDonough, W.F., 1989. Chemical and isotopic systematics of oceanic basalts: implications for mantle composition and processes. In: Saunders, A.D., Norry, M.J. (Eds.), Magmatism in Ocean Basins. Geol. Soc. London. Spec. Publ., vol. 42, pp. 313–345.

Tahirkeli, R.A.K., 1982. Geology of the Himalaya, Karakoram, and Hindu Kush in Pakistan. Geol. Bull. Univ. Peshawar Spec. Issue 11, 1–189.

Tahirkeli, R.A.K., Mattauer, M., Proust, F., Tapponnier, P., 1979. The India Eurasia suture zone in Northern Pakistan: synthesis and interpretation of recent data at plate scale. In: Farah, A., De Jong, K.A. (Eds.), Geodynamics of Pakistan. Geol. Surv. Pakistan, Quetta, pp. 125–130.

Thakur, V.C., Misra, D.K., 1984. Tectonic framework of the Indus and Shyok suture zones in eastern Ladakh (N–W Himalaya). Tectonophysics 101, 207–220.

Treloar, P.J., Rex, D.C., Guise, P.G., Coward, M.P., Searle, M.P., Windley, B.F., Petterson, M.G., Jan, M.Q., Luff, I.W., 1989. K–Ar and Ar–Ar geochronology of the Himalayan collision in NW Pakistan: constraints on the timing of suturing, deformation, metamorphism and uplift. Tectonics 8, 884–909.

Treloar, P.J., Petterson, M.G., Jan, M.Q., Sullivan, M.A., 1996. A re-evaluation of the stratigraphy and evolution of the Kohistan Arc sequence, Pakistan Himalaya: implications for magmatic and tectonic arc-building processes. J. Geol. Soc. (London) 153, 681–693.

Tu, K., Fowler, M.F.J., Carlson, R.W., Zhang, M., Xie, G., 1991. Sr, Nd, and Pb isotopic compositions of Hainan basalts (South China): implications for a subcontinental lithosphere DUPAL source. Geology 19, 567–569.

Van der Voo, R., Spakman, W., Bijwaard, H., 1999. Tethyan subducted slabs under India. Earth Planet. Sci. Lett. 171, 7–20.

Vroon, P.Z., Bergen, M.J.V., 1993. Sr–Nd–Pb Isotope Systematics of the Banda Arc, Indonesia: combined Subduction and Assimilation of Continental Material. J. Geophys. Res. 98, 22349–22366.

Vroon, P.Z., Bergen, M.J.V., Klaver, G.J., White, W.M., 1995. Strontium, neodymium, and lead isotopic and trace-element signatures of the East Indonesian sediments: Provenance and implications for Banda Arc magma genesis. Geochim. Cosmochim. Acta 59, 2573–2598.

Weinberg, R.F., Dunlap, W.J., 2000. Growth and Deformation of the Ladakh Batholith, Northwest Himalayas: implications for timing of continental collision and origin of calc-alkaline batholiths. J. Geol. 108, 303–320.

White, W.M., Hofmann, A.W., Puchelt, H., 1987. Isotope geochemistry of Pacific mid-ocean ridge basalt. J. Geophys. Res. 92, 4881–4893.

Woodhead, J.D., 1989. Geochemistry of the Mariana arc (Western Pacific): source composition and processes. Chem. Geol. 76, 1–24.

Wyllie, P.J., 1971. The role of water in magma genesis and initiation of diapiric uprise in the mantle. J. Geophys. Res. 76, 1328–1338.

Yogodzinski, G.M., Kay, R.W., Volynets, O.N., Koloskov, A.V., Kay, S.M., 1995. Magnesian andesites in the western Aleutians Komandorsy region: implications for slab melting and metasomatic processes in the mantle wedge. Geol. Soc. Am. Bull. 107, 505–519.

Zindler, A., Hart, S., 1986. Chemical geodynamics. Ann. Rev. Earth Planet. Sci. 14, 493–571.